The Plant Cell, Vol. 32: 1665–1688, May 2020, www.plantcell.org © 2020 ASPB.

Specific Recruitment of Phosphoinositide Species to the Plant-Pathogen Interfacial Membrane Underlies Arabidopsis Susceptibility to Fungal Infection[OPEN]

Li Qin,[a,1] Zhuqing Zhou,[b,1] Qiang Li,[a] Chun Zhai,[c] Lijiang Liu,[a,d] Teagen D. Quilichini,[e] Peng Gao,[f] Sharon A. Kessler,[g] Yvon Jaillais,[h] Raju Datla,[f] Gary Peng,[c] Daoquan Xiang,[e] and Yangdou Wei[a,2]

[a] Department of Biology, University of Saskatchewan, Saskatoon, Saskatchewan S7N 5E2, Canada
[b] Laboratory of Cell Biology, College of Life Science and Technology, Huazhong Agricultural University, Wuhan, Hubei 430070, China
[c] Saskatoon Research and Development Centre, Agriculture and Agri-Food Canada, Saskatoon, Saskatchewan S7N 0X2, Canada
[d] Key Laboratory of Biology and Genetic Improvement of Oil Crops, Ministry of Agriculture, Oil Crops Research Institute, Chinese Academy of Agricultural Sciences, Wuhan, Hubei 430062, China
[e] National Research Council Canada, Saskatoon, Saskatchewan S7N 0W9, Canada
[f] Global Institute for Food Security, University of Saskatchewan, Saskatoon, Saskatchewan S7N 0W9, Canada
[g] Department of Botany and Plant Pathology, Purdue University, West Lafayette, Indiana 47907
[h] Laboratoire Reproduction et Développement des Plantes, Université de Lyon, École normale supérieure de Lyon, Université Claude Bernard Lyon 1, CNRS, INRA, Lyon 69342, France

ORCID IDs: 0000-0002-1821-9946 (L.Q.); 0000-0003-1332-3928 (Z.Z.); 0000-0003-0705-2850 (Q.L.); 0000-0002-9613-8287 (C.Z.); 0000-0002-0108-0407 (L.L.); 0000-0003-3311-3776 (T.D.Q.); 0000-0002-6586-4307 (P.G.); 0000-0002-7964-0451 (S.A.K.); 0000-0003-4923-883X (Y.J.); 0000-0003-0790-5569 (R.D.); 0000-0002-9072-7187 (G.P.); 0000-0001-7144-1274 (D.X.); 0000-0001-7161-9845 (Y.W.)

Different phosphoinositides enriched at the membranes of specific subcellular compartments within plant cells contribute to organelle identity, ensuring appropriate cellular trafficking and function. During the infection of plant cells, biotrophic pathogens such as powdery mildews enter plant cells and differentiate into haustoria. Each haustorium is enveloped by an extrahaustorial membrane (EHM) derived from the host plasma membrane. Little is known about the EHM biogenesis and identity. Here, we demonstrate that among the two plasma membrane phosphoinositides in Arabidopsis (*Arabidopsis thaliana*), PI(4,5)P_2 is dynamically up-regulated at powdery mildew infection sites and recruited to the EHM, whereas PI4P is absent in the EHM. Lateral transport of PI(4,5)P_2 into the EHM occurs through a brefeldin A-insensitive but actin-dependent trafficking pathway. Furthermore, the lower levels of PI(4,5)P_2 in *pip5k1 pip5k2* mutants inhibit fungal pathogen development and cause disease resistance, independent of cell death-associated defenses and involving impaired host susceptibility. Our results reveal that plant biotrophic and hemibiotrophic pathogens modulate the subcellular distribution of host phosphoinositides and recruit PI(4,5)P_2 as a susceptibility factor for plant disease.

INTRODUCTION

Filamentous phytopathogens have evolved numerous strategies to gain nutrients from host plants, but arguably one of the most specialized among these is that of the biotrophic fungi and oomycetes, which feed only on living plant cells to support their growth and propagation. These pathogens consist of a diverse range of species from phylogenetically distinct groups: the fungal powdery mildews (ascomycetes) and rusts (basidiomycetes) and the oomycete downy mildews cause substantial economic losses in major agricultural crops and environmental destruction in natural ecosystems. A distinguishing feature of these obligate biotrophs is the formation of a feeding structure called a haustorium, which forms inside the host cell after a specialized fungal hypha penetrates the plant cell wall. The haustorium, however, remains separated from the host cell cytoplasm, surrounded by a highly modified membrane, the extrahaustorial membrane (EHM), derived from the invaginated host plasma membrane (PM; Gil and Gay, 1977; Roberts et al., 1993). Haustoria appear to play essential roles in plant-fungus recognition, uptake of nutrients into the pathogen, and delivery of secreted effector proteins into host cells for the establishment of a successful biotrophic relationship (Heath, 1997; Hahn and Mendgen, 2001; Voegele and Mendgen, 2003; Catanzariti et al., 2006; Yi and Valent, 2013; Lo Presti et al., 2015). Similar to haustoria, the biotrophic hyphae of some hemibiotrophic fungi, such as *Colletotrichum* spp and *Magnaporthe oryzae*, grow intracellularly in host tissue. The biotrophic hyphae are surrounded by an extra-invasive hyphal membrane (EIHM) contiguous with the host PM, forming a tight biotrophic interface. The biotrophic stage of hemibiotrophic fungi, without killing host cells, is a crucial step for the pathogen to initiate infection.

[1] These authors contributed equally to this work.
[2] Address correspondence to yangdou.wei@usask.ca.
The author responsible for distribution of materials integral to the findings presented in this article in accordance with the policy described in the Instructions for Authors (www.plantcell.org) is: Yangdou Wei (yangdou.wei@usask.ca).
[OPEN]Articles can be viewed without a subscription.
www.plantcell.org/cgi/doi/10.1105/tpc.19.00970

IN A NUTSHELL

Background: Biotrophic plant pathogens such as powdery mildews and rusts require living cells to feed on and they form a specialized feeding structure called the haustorium inside host cells for nutrient uptake. The haustorium is enveloped by a highly modified extrahaustorial membrane (EHM) that separates the haustorium from the cytoplasm of its host cell. Our knowledge about the biogenesis of the EHM is limited, although some models hypothesize that the EHM originates from the host plasma membrane (PM). In the Arabidopsis–powdery mildew interaction, all plant PM-localized proteins tested appear to be absent at the EHM, and the specific identity and composition of the EHM remain a mystery. Uncovering the chemical composition of EHM can help us understand the mechanisms underlying the biogenesis and function of the haustorium.

Question: Membrane identities are acquired by the combined presence of specific proteins and lipids. We tested whether the EHM has a distinct lipid profile from the PM by examining the distribution of phosphoinositide species that are partitioned in the membrane systems, thereby contributing to the membrane identity and function.

Findings: We show that among two major PM phosphoinositide species in Arabidopsis, only PI(4,5)P_2, but not PI4P, selectively targets to the EHM. The PI(4,5)P_2 content increases at the powdery mildew infection site, and the accumulation of PI(4,5)P_2 at the EHM occurs through an ectopic transport from the PM pool dependent on actin cytoskeleton-mediated cellular trafficking. Depletion of PI(4,5)P_2 by mutating its biosynthetic enzyme genes prevents disease development of host plants against various plant pathogens. Disease resistance in the mutant is not accompanied by cell death-associated immune defenses, but rather involves the loss of host susceptibility. Together, our findings reveal that plant biotrophic pathogens modulate the subcellular redistribution of host phosphoinositides and recruit PI(4,5)P_2 as a susceptibility factor for plant disease.

Next steps: This study reveals that the EHM has a distinct nature in lipid profiles from other membranes. Since both PI(4,5)P_2 and PI4P have multiple effects in regulating cellular functions, the underlying cellular mechanisms contributing to the enhanced disease resistance in the PI(4,5)P_2 biosynthetic mutants will be addressed in future work.

Although the EHM is considered by some models to be derived from the host PM, cytological studies revealed that the two membranes have distinct structure and composition (Gil and Gay, 1977; Micali et al., 2011). In Arabidopsis (*Arabidopsis thaliana*)-powdery mildew interactions, all PM-localized proteins tested appear to be absent at the EHM (Koh et al., 2005; Micali et al., 2011), while several proteins that are associated with the endomembrane system are detected at the EHM (Inada et al., 2016; Berkey et al., 2017; Kwaaitaal et al., 2017). Thus, uncovering the proteinaceous nature of the EHM challenges existing models of the origin and constitution of the EHM and provides fresh insight into understanding the cellular mechanisms underlying the biogenesis of the EHM.

Membrane identities are acquired by the combined presence of specific proteins and lipids. Biological membranes are composed of a diverse array of lipids (van Meer et al., 2008). Phosphoinositides (also known as phosphatidylinositol phosphates) are a family of anionic phospholipids that are present in minute amounts in cell membranes. Phosphoinositide species are distinctly partitioned in membranes by type and thereby contribute to organelle identity (Noack and Jaillais, 2017). The principal roles of phosphoinositides are to coordinate the complex exchange of metabolites and information across membranes, the controlled expansion or reduction of membrane area, the interaction of membranes with the cytoskeleton and intracellular organelles, and the polarized distribution of peripheral or membrane-integral proteins. In plants, five out of seven known phosphoinositides have been detected, with PI4P constituting ~80%, followed in abundance by PI(4,5)P_2, PI3P, and PI(3,5)P_2 (Heilmann and Heilmann, 2015; Noack and Jaillais, 2017). PI4P and PI(4,5)P_2 are essential lipid determinants of the PM (Hammond et al., 2012). However, remarkable differences in phosphoinositide composition can be noted between plants and animals. In plants, the major pool of PI4P appears at the PM, whereas in animals, PI4P prominently resides in the Golgi/*trans*-Golgi network compartments and to a lesser extent at the PM (Simon et al., 2014, 2016). Additionally, PI(4,5)P_2 is found in much lower abundance in plant cells than in animal cells (Munnik and Vermeer, 2010; Munnik and Nielsen, 2011). Together with the mystery concerning the origin of the EHM, little is known about the membrane lipid composition of the EHM.

In this study, by using genetically encoded biosensors for each phosphoinositide species in Arabidopsis challenged by the powdery mildew fungus *Erysiphe cichoracearum* (*Ec*), we show that among the two phosphoinositides at the PM, PI(4,5)P_2 pools were dynamically upregulated at pathogen infection sites and further integrated into the EHM, whereas PI4P maintained steady levels at the PM and was absent in the EHM. Further pharmacological intervention revealed that the dynamic movement of PI(4,5)P_2 into the EHM occurred via a brefeldin A (BFA)-insensitive but actin-dependent transport pathway. Depletion of the PM PI(4,5)P_2 pool by knockout mutation of the two major phosphatidylinositol 4-phosphate 5-kinases genes *PIP5K1* and *PIP5K2*, responsible for PI(4,5)P_2 biosynthesis at the PM in leaf tissues, prevents susceptible responses and disease development of host plants against biotrophic and hemibiotrophic fungal pathogens. Together, our results suggest that fungal pathogens modulate the subcellular distribution of host phosphoinositides during pathogenesis and adopt PI(4,5)P_2 as an essential susceptibility factor for plant disease development.

RESULTS

Differential Distribution of Phosphoinositides at the Haustorial Periphery upon Powdery Mildew Infection

Phosphoinositides are key components of cellular membrane lipids. Recently, a full set of genetically encoded biosensors for detecting PI3P, PI4P, and PI(4,5)P_2 was developed to probe the localization and partitioning of phosphoinositides within the cells and tissues of stable transgenic Arabidopsis lines (Vermeer et al., 2006, 2009; van Leeuwen et al., 2007; Munnik and Nielsen, 2011; Simon et al., 2014; Platre and Jaillais, 2016). We used these well-defined biosensors to investigate the subcellular distribution of phosphoinositides in Arabidopsis plants in response to the invasion of biotrophic and hemibiotrophic fungal pathogens.

Initially, we examined the subcellular localization of PI3P, PI4P, and PI(4,5)P_2 in leaves of transgenic Arabidopsis plants expressing mCITRINE (mCIT)-tagged variants of the biosensors mCIT-2xFYVE^{HRS}, mCIT-2xPH^{FAPP1}, and mCIT-1xPH$^{PLC\delta1}$, respectively (Simon et al., 2014), upon inoculation with the biotrophic powdery mildew fungus, *Ec*. PI3P was previously shown to localize in late endosomes/prevacuolar compartments and to a lesser extent to the tonoplast in plant cells (Simon et al., 2014). Upon infection at 2 d after inoculation (DAI) with *Ec* conidiospores, confocal imaging revealed that signals for the PI3P biosensor mCIT-2xFYVE^{HRS} were detected at a distinct membrane structure surrounding the *Ec* haustorium as well as at cytosolic punctate particles likely associated with late endosomes/prevacuolar compartments (Figure 1A). The signals for mCIT-2xFYVE^{HRS} -targeted membrane formed an outer layer loosely surrounding the callosic encasement (stained by propidium iodide) of the haustorial complex and was less constricted against the haustorial peripheral surface, which suggests that PI3P is integrated into the host tonoplast rather than targeting into the EHM.

Using biosensors for PI4P and PI(4,5)P_2, the two most abundant phosphoinositides at the PM (Simon et al., 2014, 2016), confocal imaging showed that signals for the PI4P sensor mCIT-2xPH^{FAPP1} in *Ec*-infected leaf epidermal cells were associated with the PM of *Ec*-infected host cells. Furthermore, mCIT-2xPH^{FAPP1} also appeared at the outer surface of the encasement, which is covered by host PM. However, the continuous signal stopped at the haustorial neck region and was completely absent at the haustorial periphery (Figure 1B; Supplemental Figures 1A and 1B; Supplemental Movie 1). In contrast, the signal for the PI(4,5)P_2 sensor mCIT-1xPH$^{PLC\delta1}$ in *Ec*-infected leaf epidermal cells accumulated at the periphery of *Ec* haustoria likely associated with the EHM in addition to its localization at the host PM (Figure 1C; Supplemental Figures 1C and 1D; Supplemental Movie 2). Detailed spatial imaging revealed that PI(4,5)P_2 signals formed the outer and inner layers covering the surface of haustorial encasement and occasionally displayed contiguous connections between the haustorial periphery and the host PM (Supplemental Figure 1C).

To validate the distinct accumulation patterns of PI4P and PI(4,5)P_2 signals observed after *Ec* infection, we simultaneously captured PI4P and PI(4,5)P_2 signals from the same infection site using Arabidopsis plants expressing 2xCypET-1xPH^{FAPP1} and mCIT-1xPH$^{PLC\delta1}$ (Figure 1D). Indeed, the PI4P sensor was completely absent on the haustorial periphery, whereas the signal for the PI(4,5)P_2 sensor formed a peripheral layer surrounding the haustorium. Similar distribution patterns for each phosphoinositide species were observed in *Ec*-infected epidermal cells regardless of the sensors' affinity for their cognate lipid (i.e., using one or two repeats of an identical lipid binding domain) or the lipid binding domain used (i.e., mCIT-2xPH^{FAPP1}, mCIT-1xPH^{FAPP1}, and mCIT-P4M^{SiDM} for PI4P and mCIT-1xPH$^{PLC\delta1}$, mCIT-2xPH$^{PLC\delta1}$, and mCIT-1xTUBBY-C for PI(4,5)P_2; Figures 1B and 1C; Supplemental Table 1). These results indicate that various phosphoinositide biosensors provide specific, reproducible detection of distinct phosphoinositide species' subcellular localization in Arabidopsis leaf epidermal cells in association with *Ec* infection.

To independently validate that PI(4,5)P_2 is specifically recruited to the EHM, we established a protocol for whole-mount immunolocalization of PI(4,5)P_2 or PI4P in *Ec*-infected leaf epidermal cells using antibodies specifically recognizing PI(4,5)P_2 or PI4P (Hammond et al., 2006, 2009). The anti-PI(4,5)P_2 antibody labeled a membrane layer around the haustorium as well as the cell periphery (Figure 1E). Staining with anti-PI4P antibody produced the intracellular punctate signals likely corresponding to Golgi in leaf epidermal cells (Figure 1E). As shown in an earlier study using the same anti-PI4P antibody, a punctate signal was also observed in root epidermal cells (Tejos et al., 2014). This localization pattern was somewhat unexpected, considering that signals for PI4P biosensors localize primarily to both the PM and the Golgi apparatus (Figure 1B; Vermeer et al., 2009). However, it is known that different conditions are required for the preservation of PM and Golgi, and the immunofluorescence protocol for PI4P detection adapted from a previous study likely preserves Golgi staining opposed to those best for PM staining (Capasso and D'Angelo, 2019). Nevertheless, no distinct locations of anti-PI4P signals were detected surrounding the haustorial periphery (Figure 1E). No specific labeling was observed in the negative control processed without the primary antibodies. Thus, the immunofluorescence data corroborate the localization patterns of PI(4,5)P_2 and PI4P at the haustorial periphery, as revealed by the biosensors in *Ec*-infected Arabidopsis cells.

PI(4,5)P_2, but Not PI4P, Is Selectively Targeted to the EHM

The haustorium is typically surrounded by a series of subcellular compartment layers, including, from innermost to outermost: (1) the extrahaustorial matrix, (2) the EHM, (3) the host cytosol, and (4) the host tonoplast. The haustorial encasement often forms around the haustorial neck region, separating host cytosolic contents and the tonoplast from the haustorial surface.

To test whether PI(4,5)P_2 was selectively targeted to the EHM, we conducted a comprehensive colocalization analysis with a set of host cellular markers. Both PI3P and PI(4,5)P_2 were incorporated into distinct membranous layers at the haustorial periphery. To uncover the nature and identity of these membrane layers, we first coexpressed each of three phosphoinositide biosensors with the tonoplast marker Tono-cyan fluorescent protein (CFP; Nelson et al., 2007). At 2 DAI, the signal for the PI3P sensor mCIT-2xFYVE^{HRS} surrounding haustoria was tightly colocalized with Tono-CFP (Figures 2A and 2B), indicating that PI3P

is indeed targeted to the tonoplast. In contrast, the PI(4,5)P_2 biosensor mCIT-1xPH$^{PLC\delta1}$ did not colocalize with Tono-CFP but appeared as a distinct membrane layer between the haustorial body and the tonoplast (Figures 2A and 2B). With regard to PI4P, the signals of mCIT-2xPH^{FAPP1} were continuous along the PM and terminated at the haustorial neck region (Figures 2A and 2B). These data suggest that PI(4,5)P_2 is integrated into the EHM, while PI4P appears to be absent from the EHM.

A previous study reported that the EHM-specific marker RPW8.2-red fluorescent protein (RFP) and its homologs yellow fluorescent protein (YFP)-HR3 proteins remained attached to the haustorial complex, while the cytoplasm was pulled off the haustorial surface upon plasmolysis of powdery mildew-infected cells (Berkey et al., 2017). To test the association of PI(4,5)P_2 with the EHM, we subjected *Ec*-inoculated leaves coexpressing mCIT-1xPH$^{PLC\delta1}$ and Tono-CFP to plasmolysis. After incubating with

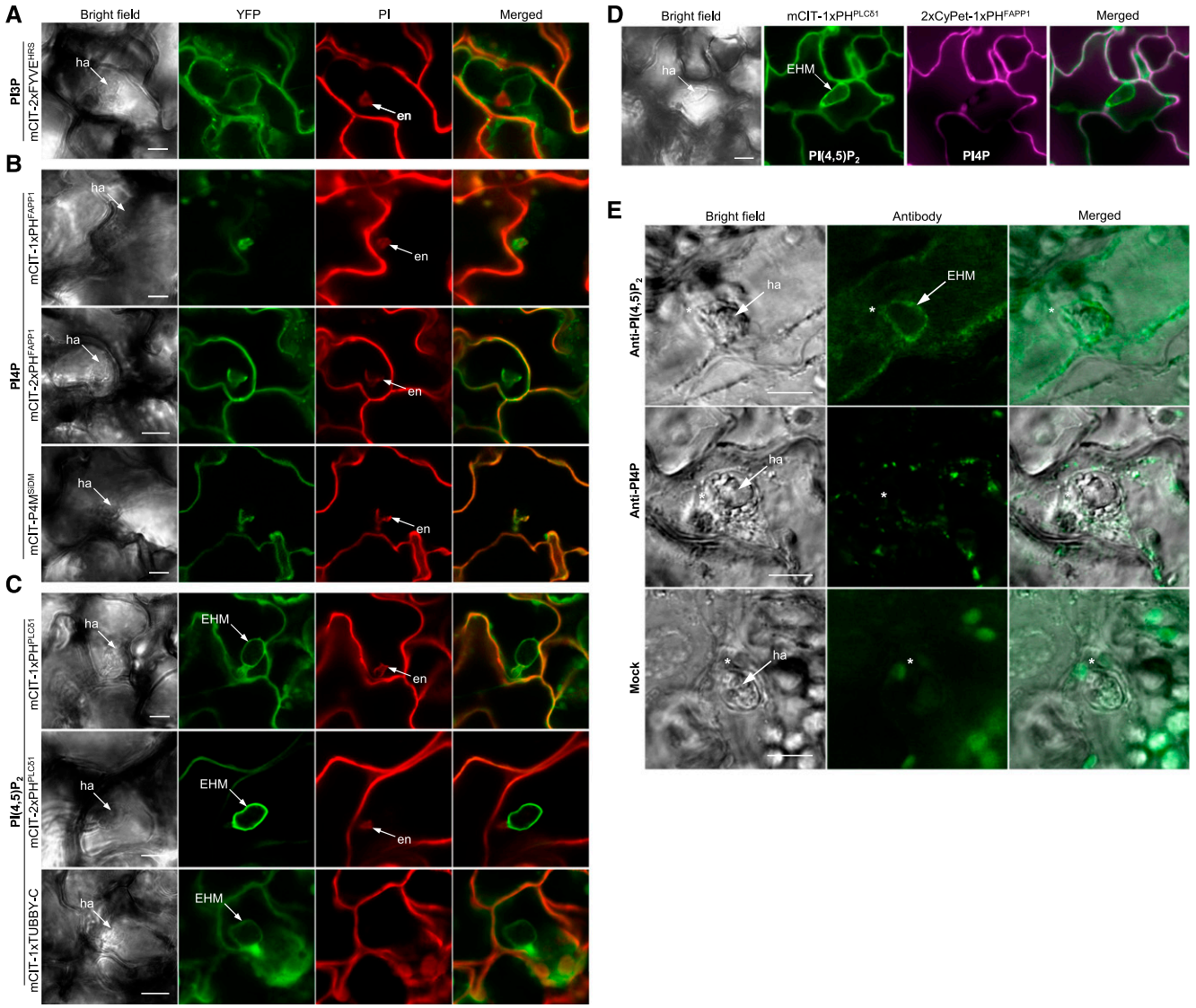

Figure 1. Differential Targeting of Phosphoinositides to the Haustorial Periphery of the Powdery Mildew *Ec*.

(A) to **(C)** Leaves of Arabidopsis plants expressing biosensors were inoculated with *Ec* and viewed with a confocal microscope at 2 DAI. Fungal structures and plant cell walls were stained with propidium iodide (PI). en, encasement; ha, haustorium. Bars = 10 μm.

(A) Representative images of PI3P biosensor mCIT-2xFYVE^{HRS}.

(B) Representative images of PI4P biosensors mCIT-1xPH^{FAPP1}, mCIT-2xPH^{FAPP1}, and mCIT-P4M^{SiDM}.

(C) Representative images of PI(4,5)P_2 biosensors mCIT-1xPH$^{PLC\delta1}$, mCIT-2xPH$^{PLC\delta1}$, and mCIT-1xTUBBY-C.

(D) Simultaneous labeling of PI(4,5)P_2 (mCIT-1xPH$^{PLC\delta1}$) and PI4P (2xCyPet-1xPH^{FAPP1}) during haustorium formation at 2 DAI. Bar = 10 μm.

(E) Immunofluorescence of *Ec*-infected leaf epidermal cells with the antibodies to PI(4,5)P_2 [anti-PI(4,5)P_2] and PI4P (anti-PI4P). Distribution of PI(4,5)P_2 and PI4P in *Ec*-infected cells was revealed by whole-mount immunolocalization of leaf epidermal tissues of Arabidopsis plants at 2 DAI. Images of mock were taken in the absence of primary antibody. Asterisks indicate *Ec* penetration sites in epidermal cells. Bars = 10 μm.

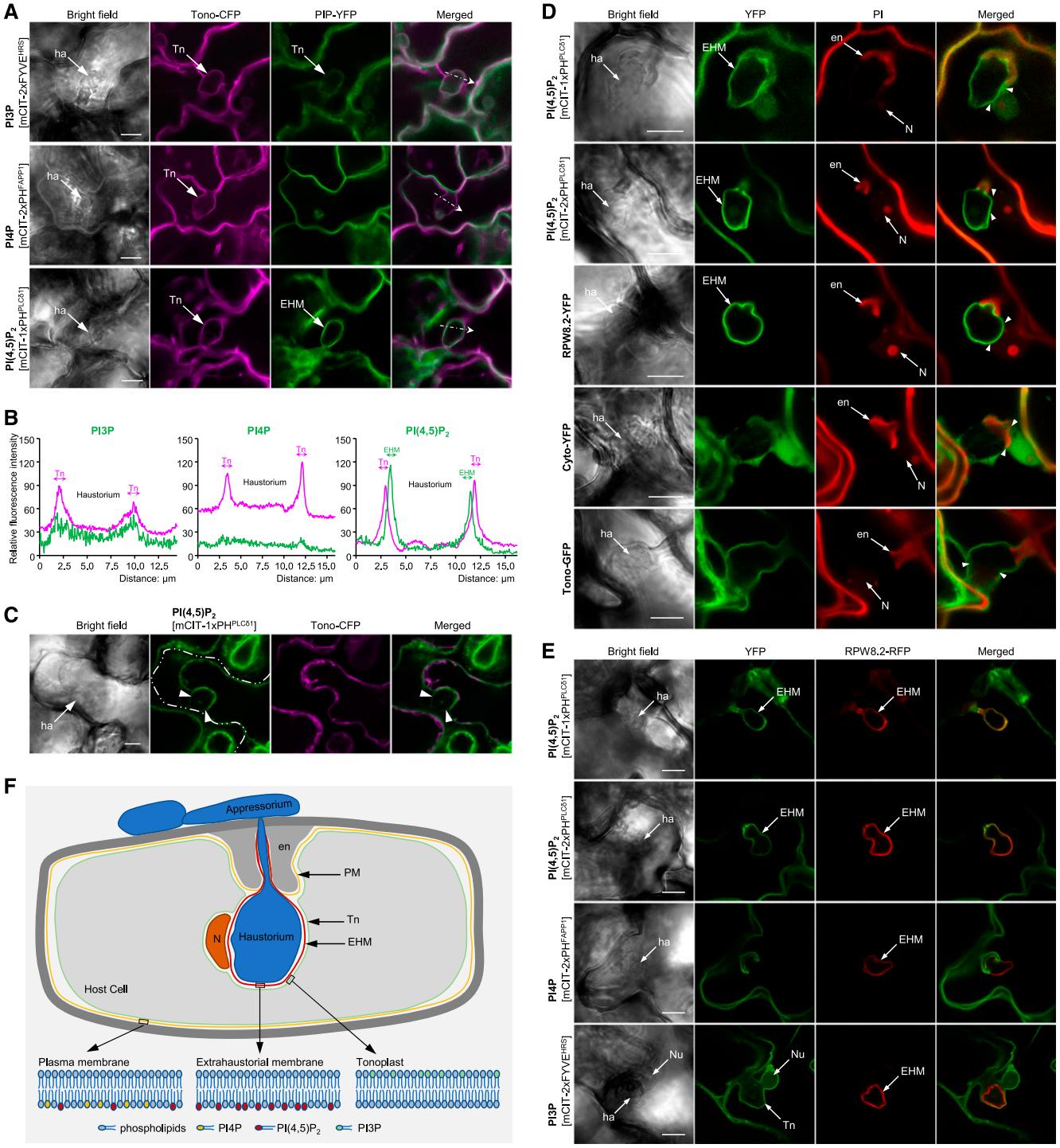

Figure 2. PI(4,5)P_2, but Not PI4P, Is Selectively Targeted to the EHM of Powdery Mildew.

(A) Representative images of *Ec*-infected Arabidopsis epidermal cells coexpressing tonoplast marker Tono-CFP and PIP biosensors mCIT-2xFYVE^{HRS} for PI3P, mCIT-2xPH^{FAPP1} for PI4P, or mCIT-1xPH$^{PLC\delta1}$ for PI(4,5)P_2 at 2 DAI. ha, haustorium; Tn, tonoplast.

(B) Plots show relative fluorescence intensity along the paths of dotted arrows in left panels corresponding to **(A)**.

(C) Arabidopsis leaves coexpressing PI(4,5)P_2 biosensor mCIT-1xPH$^{PLC\delta1}$ and Tono-CFP were inoculated with *Ec* and subjected to plasmolysis at 2 DAI. Cell walls of an infected epidermal cell are marked by a dotted line. After plasmolysis, PI(4,5)P_2 signals retained on the haustorial peripheral surface are indicated by arrowheads.

0.85 M KCl for ~30 min, the cytoplasm along with the Tono-CFP-labeled tonoplast appeared retracted from the haustorial complex, whereas the localization of mCIT-1xPH$^{PLC\delta1}$ signals at the EHM was unaffected (Figure 2C). These data support PI(4,5)P_2 localization at the EHM.

Due to the turgor pressure generated by the central vacuole in leaf epidermal cells, the cytoplasmic contents of the host cell appear to form a discontinuous layer with variable thicknesses between the EHM and the tonoplast (Koh et al., 2005). We examined the cellular distribution of a cytosolic marker (Cyto-YFP; DeBono et al., 2009) in comparison with the PI(4,5)P_2 biosensors in *Ec*-infected epidermal cells. Cyto-YFP yielded uneven, occasionally discontinuous signals surrounding the haustoria and the outer surface of the encasement (Figure 2D; Supplemental Figure 2). Furthermore, faint signals were detected at the inner side of the encasement. By contrast, both PI(4,5)P_2 probes mCIT-1xPH$^{PLC\delta1}$ and mCIT-2xPH$^{PLC\delta1}$ exhibited intense sharp layers with uniform thickness around the haustoria, and the detectable signals also appeared consistently at the inner side of the encasement (Figure 2D; Supplemental Figure 2). As revealed previously, the 1xPH$^{PLC\delta1}$ probe with a single PI(4,5)P_2 binding motif displayed a cytosolic proportion of the signals (van Leeuwen et al., 2007; Munnik and Nielsen, 2011; Simon et al., 2014), although the fluorescence intensity in the cytosol was weaker than at the PM and EHM. Notably, the probe mCIT-2xPH$^{PLC\delta1}$ with two PI(4,5)P_2 binding motifs that was demonstrated to be exclusively localized to the PM (Simon et al., 2014) showed a sharp accumulation at the EHM as well as at the PM in *Ec*-infected cells.

During the infection process, the host nucleus often moves toward the infection site of haustorium-containing cells (Inada et al., 2016; Scheler et al., 2016). We observed mCIT-1xPH$^{PLC\delta1}$ and mCIT-2xPH$^{PLC\delta1}$ signals as a distinct layer surrounding the haustorium, separating the haustorium from the nucleus, whereas no clear boundary appeared between the haustorium and its neighboring nucleus by either the Cyto-YFP-labeled cytosol or the Tono-YFP-labeled tonoplast (Figure 2D). Notably, the EHM marker RPW8.2-YFP (Wang et al., 2007, 2009) also displayed a sharp boundary layer between the haustorium and the adjacent nucleus, while the Tono-YFP-labeled tonoplast surrounded the haustorium and the nucleus (Figure 2D).

To further examine the localization of phosphoinositides in association with the EHM, we coexpressed mCIT-tagged biosensors with the EHM-specific marker RPW8.2-RFP (Wang et al., 2007). At 2 DAI, a continuous layer of both mCIT-1xPH$^{PLC\delta1}$ and mCIT-2xPH$^{PLC\delta1}$ encompassing the haustoria was tightly colocalized with RPW8.2-RFP (Figure 2E). Signals for both PI(4,5)P_2 biosensors (mCIT-1xPH$^{PLC\delta1}$ and mCIT-2xPH$^{PLC\delta1}$) as well as for RPW8.2-RFP were evident at the haustorial neck region. Further colocalization studies revealed that the PI4P biosensor mCIT-2xPH^{FAPP1} covered the encasement surface, but it was not detected from the RPW8.2-RFP-labeled EHM (Figure 2E). The PI3P biosensor mCIT-2xFYVE^{HRS} formed an additional layer outside the RPW8.2-RFP-labeled EHM, targeting to the tonoplast (Figure 2E). Taken together, these results reveal that PI4P and PI(4,5)P_2, two of the most abundant phosphoinositides at the PM in plant cells (Vermeer et al., 2009; Simon et al., 2014, 2016), are likely associated with independent lipid determinants of membrane identity, and only PI(4,5)P_2 is selectively integrated into the EHM during haustorial biogenesis (Figure 2F).

To investigate whether the distribution of phosphoinositides at the EHM was a common characteristic of the interactions between host plants and haustorium-forming pathogens, we examined the localizations of PI3P, PI4P, and PI(4,5)P_2 in leaves of Arabidopsis plants expressing corresponding biosensors upon infection with the white rust oomycete, *Albugo candida*. At 2 DAI with zoospores, confocal imaging revealed that the PI3P biosensor mCIT-2xFYVE^{HRS} formed a membrane layer enveloping the *A. candida* haustorium, likely targeting it to the host tonoplast (Supplemental Figure 3A). Similar to infection by the powdery mildew, the signals for the PI4P biosensor mCIT-2xPH^{FAPP1} discontinued at the haustorial neck region and were absent from the peripheral surface of *A. candida* haustoria (Supplemental Figure 3B). Both PI(4,5)P_2 biosensors mCIT-1xPH$^{PLC\delta1}$ and mCIT-2xPH$^{PLC\delta1}$ were recruited to the EHM of white rust (Supplemental Figure 3C). These data indicate that haustorium-forming pathogens promote the redistribution of host phosphoinositides during the infection processes, and the EHM from different host-pathogen systems has similar but unique phosphoinositide compositions.

Cellular Trafficking Pathways Responsible for the Recruitment of PI(4,5)P_2 into the EHM

To investigate the potential role of cellular trafficking pathways in the redistribution and recruitment of PI(4,5)P_2 to the EHM, we evaluated the impact of pharmacological inhibitors on the dynamic accumulation of PI(4,5)P_2 at the EHM. This involved quantification of the PI(4,5)P_2 signals at the EHM in the presence or absence of latrunculin A, oryzalin, BFA, methyl-β-cyclodextrin (MβCD), or wortmannin. Interestingly, treatment with latrunculin A, which sequesters G-actin and prevents F-actin assembly (Spector et al., 1983), led to a significant depletion of PI(4,5)P_2 from the EHM. Treatment with oryzalin, which depolymerizes microtubules (Morejohn, 1991), had no effect on PI(4,5)P_2 accumulation at the

Figure 2. (continued).

(D) Arabidopsis leaves expressing mCIT-1xPH$^{PLC\delta1}$, mCIT-2xPH$^{PLC\delta1}$, RPW8.2-YFP, Cyto-YFP, or Tono-GFP were inoculated with *Ec* and stained by propidium iodide (PI) at 2 DAI. Arrowheads indicate the boundary between the haustorium and the host nucleus (N). Cell wall, encasement (en), and nucleus were stained with propidium iodide.

(E) Representative images of *Ec*-infected Arabidopsis epidermal cells coexpressing EHM marker RPW8.2-RFP and PIP biosensors mCIT-1xPH$^{PLC\delta1}$ and mCIT-2xPH$^{PLC\delta1}$ for PI(4,5)P_2, mCIT-2xPH^{FAPP1} for PI4P, or mCIT-2xFYVE^{HRS} for PI3P at 2 DAI.

(F) Diagram illustrating the distribution of host phosphoinositide species in different membrane compartments associated with an *Ec* haustorium in infected epidermal cells.

Bars = 10 μm.

EHM (Figures 3A and 3B). Strikingly, inhibition of vesicle-mediated trafficking by BFA, which inactivates ARF-GEF GNOM activity (Geldner et al., 2003; Nielsen et al., 2012), had no significant effect on the targeting of PI(4,5)P_2 to the EHM. Treatment with MβCD, which depletes the PM sterols (Ohtani et al., 1989), resulted in significant inhibition of PI(4,5)P_2 accumulation at the EHM. We then investigated the effects of wortmannin, a well-characterized inhibitor of both PI 3-kinases and type III PI 4-kinases (Matsuoka et al., 1995; Nakanishi et al., 1995; Cutler et al., 1997; Krinke et al., 2007; Jha et al., 2018). Treatment with a high concentration of wortmannin (30 μM) caused a significant depletion of PI(4,5)P_2 at the EHM (Figures 3A and 3B). At this high concentration (30 μM), wortmannin has been shown to inhibit the function of type III PI 4-kinases, thus depleting cellular PI4P contents, although we cannot rule out that the PI3P-dependent process could contribute to the observed effect. These results indicate that the accumulation of PI(4,5)P_2 at the EHM is dependent on the formation of the actin cytoskeleton and sterols and less sensitive to GNOM-mediated vesicular transport, and the PI(4,5)P_2 pool at the EHM is likely derived from de novo synthesis from the precursor PI4P via the type III PI 4-kinases.

Spatial and Temporal Distribution of PI(4,5)P_2 Biosensors in Host Cells in Response to Infection by Powdery Mildew Fungus

To uncover PI(4,5)P_2 dynamics in host cells in response to powdery mildew attack, we examined the PI(4,5)P_2 signals in leaf epidermal cells at *Ec* invasion sites over an infection time course. Confocal imaging revealed that at an early infection stage, ~11 h post inoculation (hpi), the PI(4,5)P_2 signals aggregated near *Ec* penetration sites (Figure 4A). After successful penetration, PI(4,5)P_2 signals appeared in the EHM in the zone surrounding haustorial primordia and around fully developed haustoria.

Strong induction of PI(4,5)P_2 signals was observed in leaf epidermal cells that hosted a fully developed *Ec* haustorium and was not detected in neighboring noninfected cells (Figure 4B). High-resolution analyses revealed that induced PI(4,5)P_2 signals intensified on the peripheral surface of infected epidermal cells in association with the PM, and strong signals also sharply labeled the EHM. Both infected and noninfected epidermal cells maintained a similar level of PI(4,5)P_2 signals in the cytosol (Figure 4B). No induction of free YFP expression was detected in *Ec*-colonized

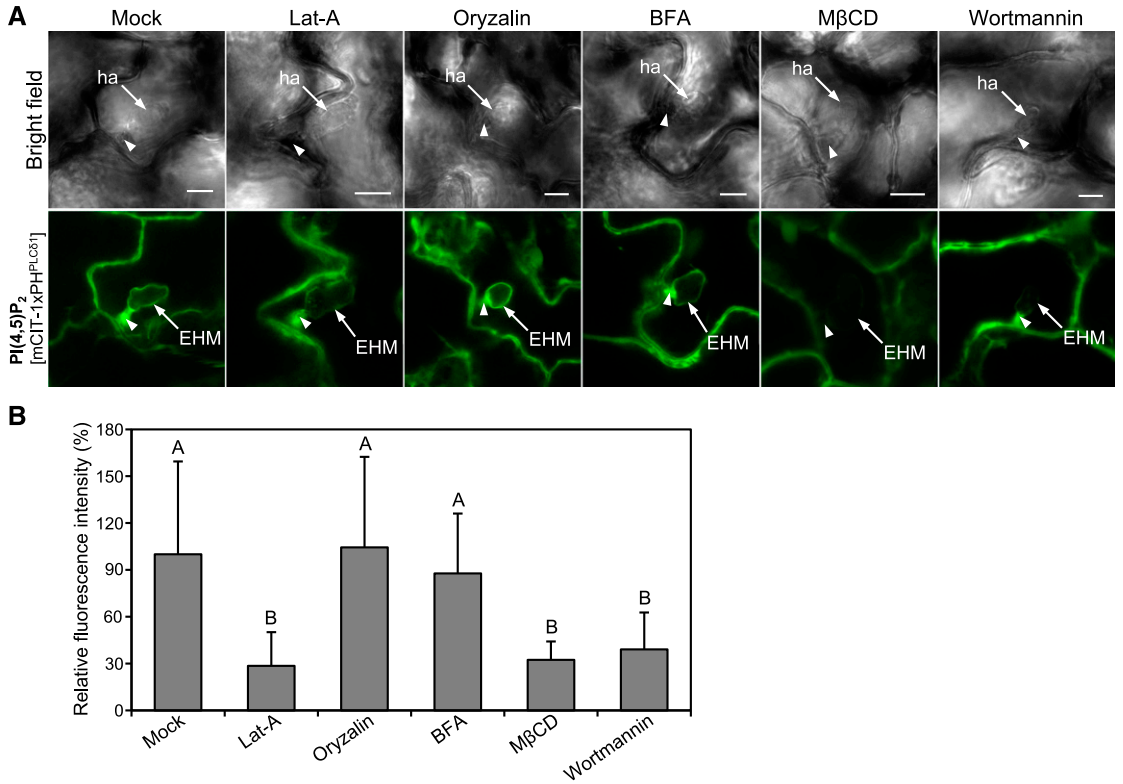

Figure 3. Cellular Trafficking Pathways Responsible for Recruiting PI(4,5)P_2 into the EHM.

Effects of pharmacological inhibitors on the targeting of PI(4,5)P_2 into the EHM are shown.

(A) Representative images showing the targeting of mCIT-1xPH$^{PLC\delta1}$ to the EHM at 24 h post *Ec* inoculation after the indicated treatments. The leaves were infiltrated with mock (water), 5 μM latrunculin A (Lat-A), 1 mM oryzalin, 300 μM BFA, 1 mM MβCD, or 30 μM wortmannin 1 h inoculation with *Ec*. The haustorial neck regions are indicated by arrowheads. ha, haustorium. Bars = 10 μm.

(B) Quantification of relative fluorescence intensity for mCIT-1xPH$^{PLC\delta1}$ at the EHM. Data are normalized over the intensity at the EHM from the mock treatment. Data are means ± SD (n = 30). Different letters indicate statistically significant differences determined by one-way ANOVA with Tukey's HSD ($P < 0.01$).

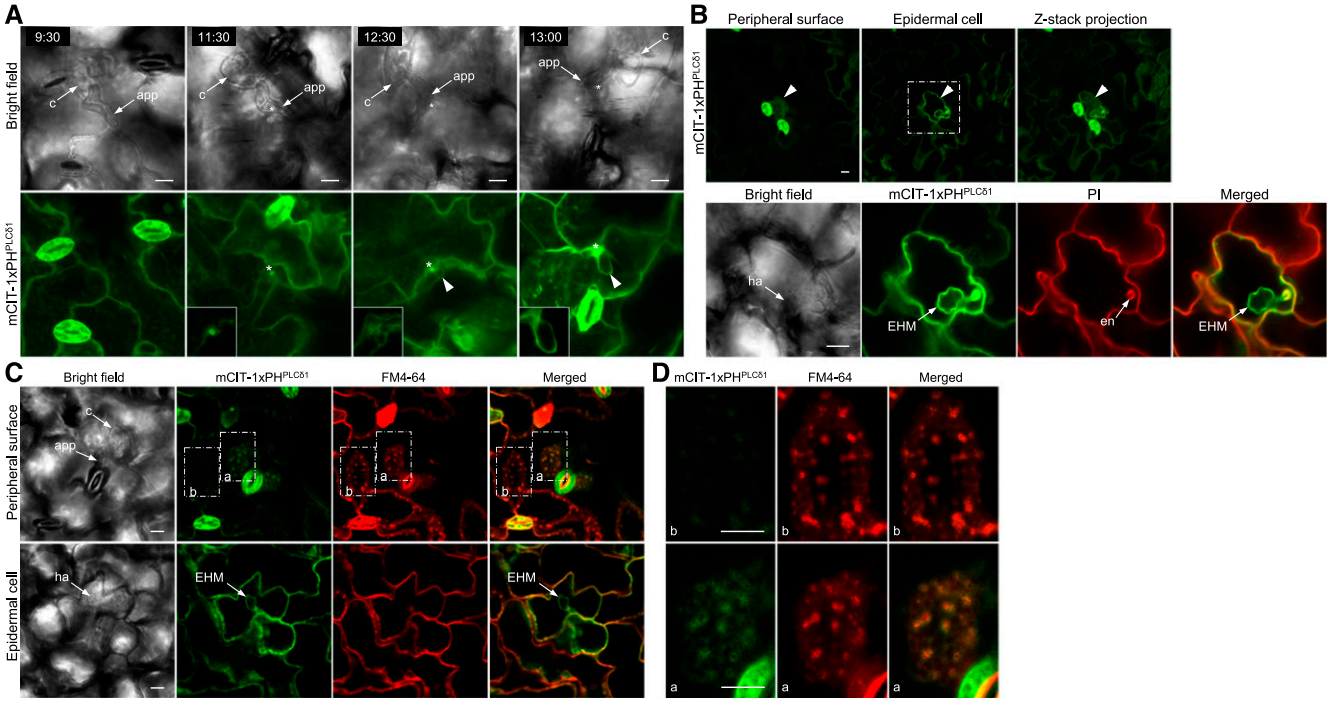

Figure 4. Induced PI(4,5)P_2 Dynamics in Host Cells in Response to Powdery Mildew Infection.

(A) Time-course responses of PI(4,5)P_2 dynamics revealed by the mCIT-1xPH$^{PLC\delta1}$ probe in *Ec*-infected epidermal cells at 9 to 14 hpi. Notably, signals of mCIT-1xPH$^{PLC\delta1}$ were focally accumulated underneath the penetration site initially at ~11 hpi and then targeted the EHM during haustorial development. Asterisks indicate the penetration sites that are enlarged in insets for close views; arrowheads indicate the EHM.

(B) Enhanced production of PI(4,5)P_2 specifically in *Ec*-colonized cells. The bottom row shows enlarged views of an *Ec*-colonized cell at 24 hpi, showing enhanced PI(4,5)P_2 signals at the EHM as well as along the PM of the infected cell. Fungal structures and plant cell walls were stained with PI. Induced accumulation was observed in 47 of 79 *Ec*-colonized cells.

(C) and **(D)** Association of induced PI(4,5)P_2 production with PM and endocytic processes in *Ec*-colonized cells. *Ec*-inoculated leaves at 24 hpi were incubated in FM4-64 for 15 min.

(C) An *Ec*-infected cell (a) and a neighboring noninfected cell (b) are highlighted in dash-lined boxes. The same inoculation sites were viewed on the peripheral surface (top) or inside the cell (bottom) of leaf epidermis.

(D) Enlarged views of an *Ec*-infected cell (a) and a noninfected cell (b). Note that PI(4,5)P_2 signal revealed by mCIT-1xPH$^{PLC\delta1}$ was induced only in the *Ec*-colonized cell and colocalized with FM4-64-labeled endocytic PM compartments on the peripheral surface of the infected cell.

app, appressorium; c, conidium; en, encasement; ha, haustorium. Bars = 10 μm.

cells compared with neighboring noninfected cells of transgenic plants expressing pUBQ10:YFP with the same promoter driving the expression of the PI(4,5)P_2 biosensor mCIT-1xPH$^{PLC\delta1}$ (Supplemental Figure 4), suggesting that the powdery mildew infection has no significant effects on *pUBQ10* promoter activity.

To examine the dynamic details of the enhanced production of PI(4,5)P_2 signals in PM, we treated *Ec*-infected leaves with FM4-64, a lipophilic styryl dye widely used as a fluorescent probe for the detection of PM internalization during endocytosis and membrane trafficking (Jelínková et al., 2010). After 15 min of stain uptake, FM4-64-labeled PM appeared as intensive aggregates in both *Ec*-infected and noninfected epidermal cells (Figures 4C and 4D). In the epidermal cells hosting haustoria, enhanced PI(4,5)P_2 signals formed amorphous accumulations that colocalized with the FM4-64-labeled aggregates, whereas the FM4-64-labeled aggregates in noninfected cells were coupled with less or no PI(4,5)P_2 signals. These results suggest that induced PI(4,5)P_2 pools in haustorium-forming cells are likely associated with enhanced PM trafficking.

PI(4,5)P_2 Production via PI4P 5-Kinases Is an Essential Susceptibility Factor in Plant-Pathogen Interactions

PI4P 5-kinase (PIP5K) converts PI4P to PI(4,5)P_2 in eukaryotes (Toker, 1998; Choi et al., 2015). The Arabidopsis genome contains genes encoding 11 isoforms of PIP5Ks that are classified into two distinct subfamilies: type A includes PIP5K10 and PIP5K11 with domain structures similar to PIP5Ks in mammals and yeasts, while type B includes isoforms PIP5K1 to PIP5K9 with additional N-terminal Lin and MORN domains (Mueller-Roeber and Pical, 2002; Heilmann and Heilmann, 2015). The Affymetrix microarray data from Genevestigator (https://www.genevestigator.com; Hruz et al., 2008) revealed that *PIP5K1*, *-2*, *-3*, *-7*, *-8*, *-9*, and *-11* were expressed at varying but substantial levels in rosette leaves, especially in mature leaves (Supplemental Figure 5A). To validate the microarray data and to identify which isoform(s) of PIP5K contributes to PI(4,5)P_2 production upon powdery mildew attack, we employed RT-PCR analysis for expression profiling of *PIP5K*

isoforms in Arabidopsis leaves with or without *Ec* inoculation (Supplemental Figure 5B). RT-PCR results showed detectable expression of *PIP5K1*, *-2*, *-5*, *-7*, *-8*, and *-9* in mature Arabidopsis leaves. Among those, *PIP5K1* and *PIP5K2* were constitutively expressed at high levels. The expression of *PIP5K8* was slightly induced by *Ec* infection compared with noninoculated leaves.

To elucidate the function of the kinases encoded by expressed *PIP5K* genes in Arabidopsis-powdery mildew interactions, we undertook a reverse genetic approach employing T-DNA insertion mutants for pathogenicity tests. We obtained and confirmed homozygous T-DNA mutant lines for *PIP5K1* (SALK_146728), *PIP5K2* (SALK_012487), *PIP5K5* (SALK_147475), *PIP5K7* (SALK_151429), *PIP5K8* (SAIL_561_F09), and *PIP5K9* (WiscDsLox434B6; Supplemental Figure 5C). Since both *PIP5K1* and *PIP5K2* showed high levels of expression in Arabidopsis mature leaves, and recombinant PIP5K1 and PIP5K2 displayed the highest catalytic activities in vitro among ubiquitously expressed PIP5Ks from Arabidopsis (Supplemental Figures 5A and 5B; Stenzel et al., 2008; Ischebeck et al., 2013;), we generated the double mutant *pip5k1 pip5k2* by crossing the respective single insertion lines. As described previously, the *pip5k1 pip5k2* double mutant exhibited reduced growth in the seedling and rosette stages, characterized by reduced leaf expansion and slow growth (Supplemental Figure 6; Ischebeck et al., 2013; Tejos et al., 2014). The triple (*pip5k1 pip5k2 pip5k5* and *pip5k1 pip5k2 pip5k8*) and quadruple (*pip5k1 pip5k2 pip5k5 pip5k8*) mutants were generated by crossing a single mutant (*pip5k5* or *pip5k8*) with the double mutant (*pip5k1*$^{-/-}$ *pip5k2*$^{-/+}$). The triple and quadruple mutants showed similar phenotypes to the double mutant, but the triple (*pip5k1 pip5k2 pip5k8*) and quadruple (*pip5k1 pip5k2 pip5k5 pip5k8*) mutants displayed enhanced growth defects (Supplemental Figure 6). These results indicate that the expressed *PIP5K* genes exhibit partially redundant and additive roles in Arabidopsis vegetative growth and development, with *PIP5K1* and *PIP5K2* playing the most predominant functions.

When challenged with *Ec*, all single mutants supported wild-type levels of hyphal growth, and *Ec* was able to sporulate at 7 DAI (Figures 5A and 5B; Supplemental Figure 5D). In contrast, *Ec* growth and development were severely impaired on the *pip5k1 pip5k2* double mutant (Figures 5A and 5B; Supplemental Figure 5D). On the mature leaves of *pip5k1 pip5k2*, *Ec* displayed a remarkably lower penetration rate and formed smaller colonies with statistically significant reduction in second hypha length and branches, total haustorial numbers per colony, and total conidiophores per colony (Figures 5C to 5I). The triple (*pip5k1 pip5k2 pip5k5* and *pip5k1 pip5k2 pip5k8*) and quadruple (*pip5k1 pip5k2 pip5k5 pip5k8*) mutants exhibited similar levels of disease severity after *Ec* infection to the double mutant (Figures 5A and 5B). Thus, among the highly expressed *PIP5K* genes in leaf tissues, *PIP5K1* and *PIP5K2* play predominant functions in powdery mildew susceptibility, and disruption of both genes renders knockout mutants highly resistant to the compatible powdery mildew fungus.

We further examined plant susceptibility to a second biotrophic phytopathogen, the white rust oomycete *A. candida* (isolate Acem1), and pathogenicity assays were conducted on the double, triple, and quadruple *pip5k* mutants. After inoculation with zoospores, abundant white blisters surrounding the inoculation sites were observed on the abaxial surface of wild-type leaves at 10 to 15 DAI (Supplemental Figure 7). At the same inoculation stages, no visible symptoms appeared on leaves of the double, triple, and quadruple mutants (Supplemental Figure 7), indicating that these mutants gained strong resistance to *A. candida*.

The impact of disruption of *PIP5K1* and *PIP5K2* genes on the cellular dynamics of PI(4,5)P_2 was further investigated in leaf epidermal cells of the mutant with or without *Ec* inoculation. We introduced the PI(4,5)P_2 biosensor mCIT-1xPH$^{PLC\delta1}$ into the *pip5k1 pip5k2* mutant and examined the fluorescence intensity at the PM. Quantitative imaging revealed that the mCIT-1xPH$^{PLC\delta1}$ signal intensity at the PM was significantly reduced in the mutant compared with wild-type plants (Supplemental Figures 8A and 8B). RT-PCR revealed that the wild type and the *pip5k1 pip5k2* mutant expressed comparable levels of the *mCIT-1xPH$^{PLC\delta1}$* transcripts (Supplemental Figure 8C), indicating that reduced levels of mCIT-1xPH$^{PLC\delta1}$ signal intensity in the *pip5k1 pip5k2* mutant were not due to transgene silencing. At the PM of wild-type leaf epidermal cells, the clustered signals from PI(4,5)P_2 biosensors coalesced, forming distinct microdomains. However, this characteristic distribution of PI(4,5)P_2 was substantially diminished in the PM of the *pip5k1 pip5k2* mutant (Supplemental Figure 8A). Together, these data indicate that isoforms PIP5K1 and PIP5K2 are key members of the Arabidopsis PIP5K family and are required to maintain the PM pool of PI(4,5)P_2 in leaf epidermal cells.

Furthermore, when challenged with *Ec*, the relative fluorescence intensity of mCIT-1xPH$^{PLC\delta1}$ at the EHM was dramatically reduced in *Ec*-infected epidermal cells of *pip5k1 pip5k2* compared with the wild type (Supplemental Figure 8D), suggesting that targeting of PI(4,5)P_2 to the EHM was impaired in the mutant. Interestingly, although the PI(4,5)P_2 signals were significantly reduced at the PM and EHM in epidermal cells of *pip5k1 pip5k2*, the epidermal cell hosting *Ec* haustoria still displayed stronger PI(4,5)P_2 signals than that of adjacent noninfected epidermal cells (Supplemental Figure 8E). This observation suggests that other isoform(s) of the PIP5K family rather than PIP5K1 and PIP5K2 are likely involved in the induction of PI(4,5)P_2 pools in the *Ec*-infected epidermal cells, although we could not exclude the possible prevention of PI(4,5)P_2 degradation that may occur in the *Ec*-infected epidermis.

Since PIP5K1 and PIP5K2 are predominantly responsible for replenishing the PI(4,5)P_2 pools in the PM of epidermal cells and at the EHM, we next tested whether the in situ localization of PIP5K1 and PIP5K2 directly contributes to the biosynthesis of PI(4,5)P_2 at the location. We generated transgenic Arabidopsis plants expressing *PIP5K1:PIP5K1-YFP* and *PIP5K2:PIP5K2-YFP* to enable cellular visualization of the kinase enzymes. After introducing the *PIP5K1:PIP5K1-YFP* and *PIP5K2:PIP5K2-YFP* transgenes into *pip5k1 pip5k2*, we found that ectopic expression of either construct could rescue the retarded growth phenotype of the *pip5k1 pip5k2* mutant (Supplemental Figure 6). These data indicate that the stable transgenic expression of *PIP5K1-YFP* and *PIP5K2-YFP* produced fully functional kinases. In leaf epidermal cells, both PIP5K1-YFP and PIP5K2-YFP localized predominantly at the PM (Supplemental Figures 9A and 9B), resembling the localization patterns found in root cells (Ischebeck et al., 2013; Tejos et al., 2014). Upon *Ec* attack, PIP5K1-YFP and PIP5K2-YFP

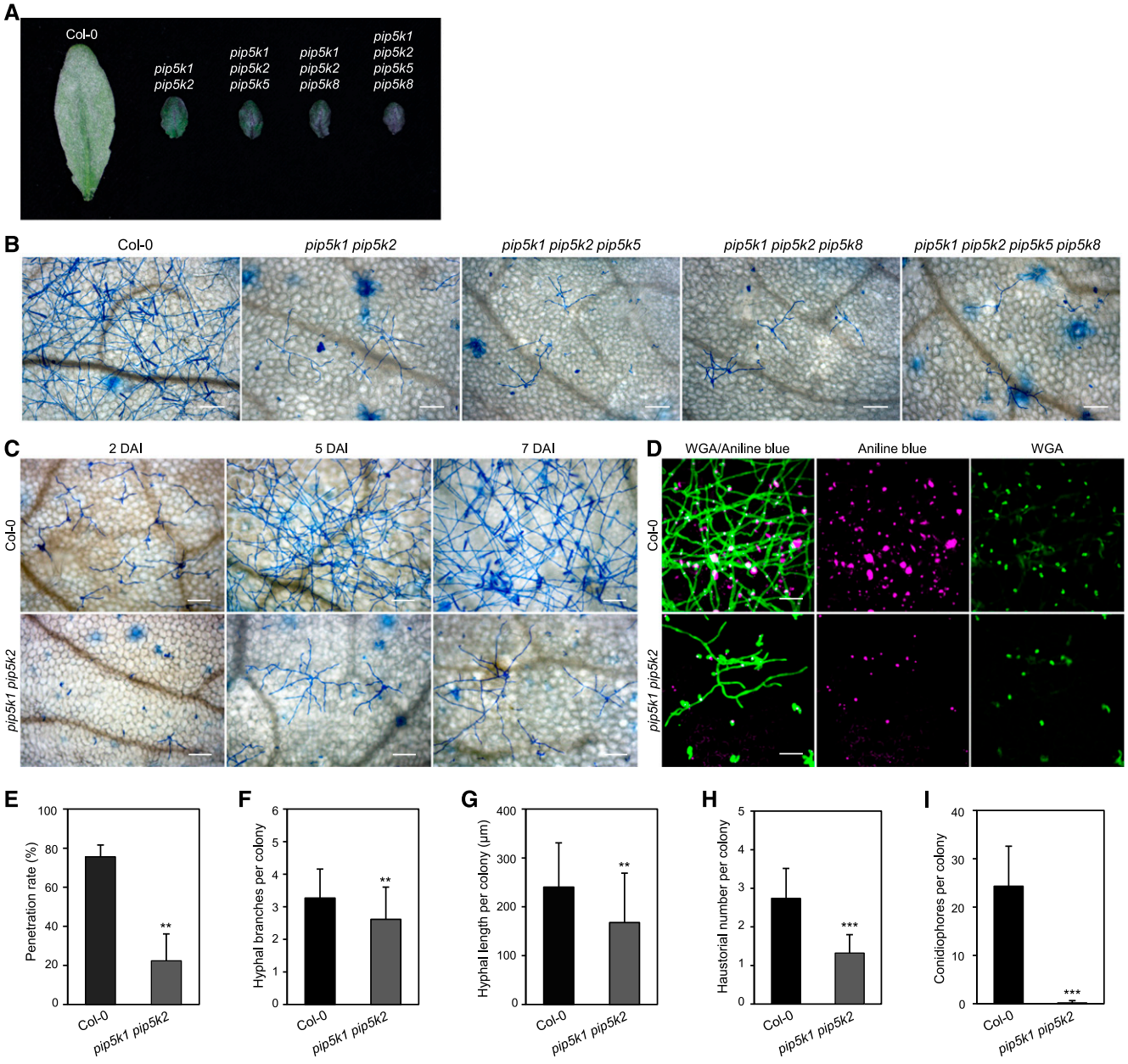

Figure 5. Loss of PIP5K1 and PIP5K2 Functions Prevented Growth and Development of the Compatible Powdery Mildew Fungus.

(A) Macroscopic infection phenotypes of double (*pip5k1 pip5k2*), triple (*pip5k1 pip5k2 pip5k5* and *pip5k1 pip5k2 pip5k8*), and quadruple (*pip5k1 pip5k2 pip5k5 pip5k8*) mutant plants at 10 DAI with *Ec*.

(B) Impaired growth and development of *Ec* on the indicated genotypes at 7 DAI with *Ec*. Leaf tissues were stained with aniline blue and viewed by light microscopy. Bars = 100 μm.

(C) Time course showing the development of *Ec* on mature leaves of the *pip5k1 pip5k2* mutant. Leaf tissues of wild-type and *pip5k1 pip5k2* plants at 2, 5, and 7 DAI were stained with aniline blue and viewed by light microscopy. Bars = 100 μm.

(D) Reduced formation of haustoria in mutant *pip5k1 pip5k2*. Fungal structures on the leaf surfaces (left) and haustoria in epidermal cells (right) at 7 DAI were stained with Alexa Fluor 488-conjugated wheat germ agglutinin (WGA), while callose deposition (middle) was detected by aniline blue. Images were taken with a confocal microscope with maximum projection of Z-stacks. Bars = 50 μm.

(E) to **(I)** Quantitative analysis of *Ec* growth on leaves of wild-type and *pip5k1 pip5k2* plants. **, $P < 0.01$ and ***, $P < 0.001$, Student's *t* test.

(E) Penetration rate of *Ec*. More than 100 sites for each leaf were scored at 2 DAI. Data are means ± SD ($n = 4$).

(F) and **(G)** Branch numbers **(F)** and total lengths **(G)** of secondary hyphae per colony at 2 DAI. Data are means ± SD ($n = 75$ [wild type] or 31 [*pip5k1 pip5k2*]).

(H) Haustorial numbers per colony at 2 DAI. Data are means ± SD ($n = 31$ [wild type] or 31 [*pip5k1 pip5k2*]).

(I) Number of conidiophores per colony at 7 DAI. Conidiophores were counted from at least 30 colonies in five leaves for each genotype, which was repeated three times with similar results. Data are means ± SD ($n = 30$).

accumulated at *Ec* penetration sites around the haustorial neck region. Noticeably, no detectable signals of PIP5K1-YFP or PIP5K2-YFP could be observed at the EHM (Supplemental Figures 9C and 9D). These results suggest that the PIP5K1 and PIP5K2 kinases generate PI(4,5)P_2 at the PM, whereas PI(4,5)P_2 at the EHM results from the lateral transport of preexisting PM pools to the EHM.

Mechanisms Underlying Powdery Mildew Resistance in the *pip5k1 pip5k2* Mutant

The enhanced resistance to biotrophic pathogen infection observed in the *pip5k1 pip5k2* double mutant suggests that underlying mechanisms may support disease resistance. To elucidate the potential mechanism(s) contributing to powdery mildew resistance in *pip5k1 pip5k2*, we examined the expression of defense-associated genes in response to powdery mildew infection by whole-transcriptome shotgun sequencing (RNA-seq). Analysis of the differentially expressed genes revealed that some of the genes involved in jasmonic acid (JA) biosynthesis, signaling, and response, such as *12-OXOPHYTODIENOATE REDUCTASE3*, *CYP82C2*, *CYP94C1*, *ALLENE OXIDE SYNTHASE*, *MYC4*, and *ETHYLENE RESPONSE FACTOR1*, displayed constitutively higher expression in the *pip5k1 pip5k2* mutant than in the wild type under the noninoculated condition. However, upon *Ec* inoculation, the majority of these genes in *pip5k1 pip5k2* showed downregulation in comparison with wild-type expression levels (Figure 6A; Supplemental Data Set 1). Thus, the JA signaling and defense pathway's role in mediating the enhanced resistance of *pip5k1 pip5k2* plants to the powdery mildew infection appears negligible.

In contrast, the expression of salicylic acid (SA)-associated defense-responsive genes, such as *PR1* and *PR2*, was significantly higher in the *pip5k1 pip5k2* mutant than in the wild type under the *Ec*-inoculated condition (Figure 6A; Supplemental Figure 10; Supplemental Data Set 1). However, a full set of genes known to be involved in SA biosynthesis and signaling were coordinately downregulated in the *pip5k1 pip5k2* mutant compared with the wild type (Figure 6A). Measurement of SA and JA contents in leaf tissues without pathogen inoculation revealed no significant differences between the wild type and *pip5k1 pip5k2*. Upon powdery mildew infection at 5 DAI, SA levels increased in infected leaves of the wild type and *pip5k1 pip5k2* but were much lower in *pip5k1 pip5k2* (Figures 6B and 6C). Collectively, these results suggest that the SA-independent defense reactions with induction of a set of *PR* genes underlie the enhanced resistance of the *pip5k1 pip5k2* mutant against powdery mildew infection.

The microbe-associated molecular patterns (MAMPs) or pathogen-associated molecular patterns have been shown to activate early-defense signaling and responses and induce the expression of MAMP-specific marker genes (Asai et al., 2002; He et al., 2006; Boudsocq et al., 2010). Our RNA-seq data revealed that although the expression of MAMP-specific marker genes, such as *FLG22-INDUCED RECEPTOR-LIKE KINASE1* (*FRK1*), *NDR1/HIN1-LIKE10*, *CYP81F2*, *WALL-ASSOCIATED KINASE2*, and *FAD-LINKED OXIDOREDUCTASE*, was coordinately induced in the *pip5k1 pip5k2* mutant upon powdery mildew attack, the expression levels of these genes remained lower than in the *Ec*-attacked wild type (Figure 6A; Supplemental Figure 10; Supplemental Data Set 1). These findings suggest that MAMP-triggered immunity is unlikely to contribute to the increased resistance of *pip5k1 pip5k2* plants.

On mature *pip5k1 pip5k2* mutant leaves, successfully penetrated *Ec* displayed remarkably retarded growth, producing significantly smaller colonies than those on wild-type leaves (Figure 5). We determined whether the resistance in *pip5k1 pip5k2* is mediated by basal defense responses by staining infected leaves with aniline blue to highlight callose deposition, a sensitive cellular marker for basal defense responses (Hauck et al., 2003). In wild-type and *pip5k1 pip5k2* plants, callose deposition was detected only at *Ec* penetration sites at 2 DAI, whereas *edr1*, a mutant that is constitutively primed for SA-inducible defenses and associated with cell death at powdery mildew infection sites (Frye and Innes, 1998), displayed enhanced callose depositions in *Ec*-infected epidermal cells that underwent accelerated cell death during infection (Figure 6D). Resistance triggered in *edr1* mutants was also associated with enhanced H_2O_2 accumulation and autofluorescence at *Ec*-infected epidermal cells (Figures 6E and 6F). In contrast, wild-type and *pip5k1 pip5k2* plants showed similar patterns of H_2O_2 production and autofluorescence on *Ec*-colonized leaves. No apparent cell death accompanied by enhanced callose deposition, H_2O_2 accumulation, and autofluorescence was observed in infected epidermal cells underneath fungal colonies on *pip5k1 pip5k2* or wild-type plants (Figures 6D to 6F). Thus, we conclude that the resistance in *pip5k1 pip5k2* to the powdery mildew fungus is not due to pathogen-triggered cell death-associated responses; rather, it may depend on reduced host susceptibility.

MLO (Mildew Locus O), a protein with seven transmembrane domains reminiscent of a G-protein-coupled receptor, is a conserved susceptibility factor to various powdery mildew species present on dicot and monocot plants (Consonni et al., 2006). It has been shown that the MLO proteins in barley (*Hordeum vulgare*) leaves focally accumulate beneath powdery mildew penetration sites coincident with the initiation of pathogen entry into host cells (Bhat et al., 2005). In Arabidopsis, the three coorthologs (*AtMLO2*, *AtMLO6*, and *AtMLO12*) of barley *MLO* are partially functionally redundant, with a predominant role for *AtMLO2* in the establishment of compatibility with the powdery mildew fungus (Consonni et al., 2006). We used transgenic lines expressing MLO2-GFP (Jones et al., 2017) to investigate the spatial and temporal dynamics of MLO2 proteins at *Ec* penetration sites. In leaf epidermal cells without *Ec* challenge, most of the MLO2-GFP fusion proteins localized at the cellular periphery as well as at cytoplasmic punctate structures that have previously been shown to colocalize with the Golgi marker Man49-mCherry (Supplemental Figure 11A; Jones et al., 2017). Upon challenge with *Ec*, a striking focal accumulation of the fusion protein appeared beneath fungal penetration sites at ~11 hpi (Figure 7A). Polarized MLO2-GFP accumulation at the *Ec* penetration site appeared to be independent of actin cytoskeleton function, since disruption of the actin cytoskeleton by latrunculin A had a negligible impact on MLO2-GFP accumulation (Figures 7B and 7C), consistent with previous findings (Bhat et al., 2005). Remarkably, at 12 to 13 hpi, coincident with host cell penetration, most MLO2-GFP proteins aggregated to *Ec* penetration sites, resulting in dramatic signal

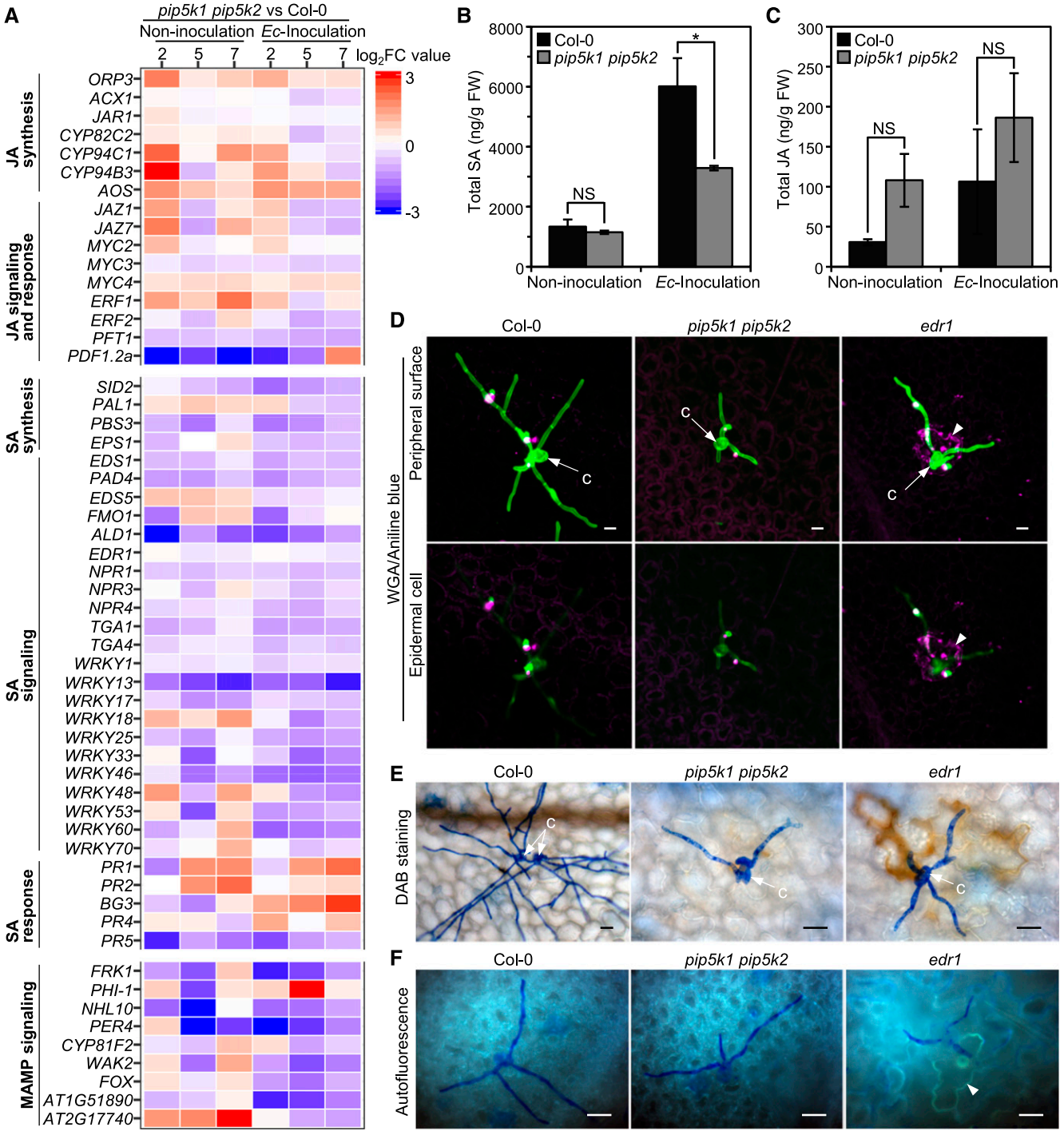

Figure 6. Defense Responses in *pip5k1 pip5k2* Mutants against Powdery Mildew Infection.

(A) Transcriptomic profiling of differentially expressed genes in SA and JA biosynthesis, signaling and response pathways, and MAMP signaling between *pip5k1 pip5k2* mutant and Col-0 plants without or with *Ec* inoculation at 2, 5, and 7 DAI. Heat maps display $\log_2$ fold change ($\log_2$FC) values for pairwise comparison between the *pip5k1 pip5k2* mutant and Col-0 at each time point.

(B) and **(C)** Levels of SA and JA in Col-0 and the *pip5k1 pip5k2* mutant. Total amounts of SA **(B)** and JA **(C)** were measured in leaf tissues without or with *Ec* inoculation at 5 DAI. Data are means ± SD ($n = 3$ biological replicates). *, $P < 0.05$; NS, no significant difference, Student's *t* test. FW, fresh weight.

(D) to **(F)** Detection of callose deposition, H_2O_2 accumulation, and autofluorescence material production in *Ec*-infected Col-0, *pip5k1 pip5k2*, and *edr1* plants at 48 hpi. Arrowheads indicate cell death in the *edr1* mutant accompanied by callose deposition, H_2O_2 accumulation, and autofluorescence. c, conidia. Bars = 20 μm.

quenching specifically within infected cells (Figure 7A; Supplemental Figure 11A). However, after successful penetration of *Ec* at ~14 hpi, the distribution of cytoplasmic MLO2-GFP in *Ec*-infected cells resumed similar patterns to the surrounding non-infected cells (Supplemental Figure 11A), and at the *Ec* penetration sites, MLO2-GFP proteins were incorporated into extracellular encasements surrounding the neck region of haustoria (Supplemental Figure 11B).

To examine whether the dynamic response and function of MLO2 is involved in modulating *Ec* penetration in the *pip5k1 pip5k2* mutant, we introduced the MLO2-GFP transgene into *pip5k1 pip5k2* plants. At 11 to 14 hpi, when the *Ec* attempted penetration failed to develop haustoria in *pip5k1 pip5k2* epidermal cells, focal accumulation of MLO2-GFP was greatly reduced or abolished beneath the *Ec* penetration sites (Figures 7A; Supplemental Figure 11C), whereas where the fungus occasionally penetrated into epidermal cells, strong focal accumulation of MLO2-GFP proteins was detected surrounding the penetration sites, despite the similar levels of the *MLO2-GFP* transcripts in wild-type and *pip5k1 pip5k2* plants (Supplemental Figure 11D). Taken together, these findings demonstrate that a rapid, transient recruitment of MLO2 proteins into the fungal invasion site correlates with successful fungal penetration, and in the *pip5k1 pip5k2* mutant, an absence of focal accumulation of MLO2-GFP at the fungal penetration site correlates with the penetration failure of the powdery mildew fungus.

In eukaryotic cells, PI(4,5)P_2 is critical for the assembly and organization of actin filaments (AFs; Moseley and Goode, 2006; Pollard, 2007). We next examined the potential impact of altered PI(4,5)P_2 levels in the *pip5k1 pip5k2* mutant on AF organization and dynamics upon *Ec* invasion. In noninoculated wild-type plants expressing GFP-ABD2-GFP, which permits the acquisition of highly resolved AF images (Wang et al., 2008), cortical AFs labeled by GFP-ABD2-GFP appeared to be branched and randomly oriented, forming a dense meshwork along the surface of the outer periclinal and anticlinal cell walls of leaf pavement cells (Supplemental Figure 11E). In contrast, cortical AFs in *pip5k1 pip5k2* cells were remarkably thinner and showed less branching than those in the wild type, and they tended to form disorganized bundles. The results demonstrate that depletion of PM PI(4,5)P_2 leads to diminished AF assembly and defects in AF organization. Upon powdery mildew attack at 12 hpi, fine AFs in wild-type epidermal cells formed an intense network surrounding the pathogen's attempted penetration site, whereas in *pip5k1 pip5k2* cells, no distinct AF network appeared underneath fungal penetration sites, and AFs were preferentially organized into thick parallel bundles radiating across epidermal cells toward the infection site (Figure 7D). After the fungus successfully penetrated into epidermal cells, static and dense AFs, but not microtubules, closely surrounded developing haustoria in wild-type epidermal cells at 20 hpi (Figures 7E and 7F).

At the same infection stage in *pip5k1 pip5k2* mutants, GFP-ABD2-GFP exhibited relatively high levels of diffuse cytoplasmic fluorescence compared with that of the wild type, and AFs were barely visible on the surface of developing haustoria (Figure 7E). At 7 DAI, powdery mildew infection resulted in rapid colony development and fungal sporulation on the surface of wild-type leaves, and within the epidermal cells hosting mature haustoria, abundant thick AF bundles were highly dynamic and frequently arrayed from the surface of mature haustorium toward the cortical region of the cells (Figure 7G; Supplemental Movie 3). In the *pip5k1 pip5k2* mutant, AF bundles in *Ec*-infected cells dispersed in connection with the *Ec* infection site, showing reduced cohesive attachment to the haustorial surface (Figure 7G; Supplemental Movie 4). The impaired AF network at the fungal penetration site as well as on the haustorial surface suggests that *pip5k1 pip5k2* mutants displayed reduced actin-dependent cellular processes underlying the Arabidopsis-powdery mildew interaction.

PI(4,5)P_2 Acts as a Susceptibility Factor for the Non-Haustorium-Forming Hemibiotroph *Colletotrichum higginsianum*

The crucifer anthracnose fungal pathogen *Colletotrichum higginsianum* (*Ch*) displays a multistage hemibiotrophic infection strategy on host Arabidopsis (Liu et al., 2007b). The pathogen invades Arabidopsis plants through direct penetration of host cell walls, forming invasive primary hyphae in epidermal cells. Following a brief biotrophic phase, the large primary hyphae switch to thin necrotrophic secondary hyphae that are associated with necrotic lesion development (Liu et al., 2007b). Similar to haustoria, the biotrophic hyphae of *Colletotrichum* spp. are completely encased by a specialized membrane structure, known as the EIHM. The specialized EIHM has been suggested to resemble the functionality of the EHM in haustorium-forming biotrophs (Lo Presti et al., 2015).

To determine the distribution of PI4P and PI(4,5)P_2 in association with the EIHM, plants expressing respective biosensors, mCIT-2xPH^{FAPP1} and mCIT-1xPH$^{PLC\delta1}$, were inoculated with *Ch* and examined by confocal microscopy. Remarkably, signals for both PI4P biosensor mCIT-2xPH^{FAPP1} and PI(4,5)P_2 biosensors mCIT-1xPH$^{PLC\delta1}$ and mCIT-2xPH$^{PLC\delta1}$ were located around the infection vesicles and primary hyphae, where the enrichment of PI(4,5)P_2 biosensor mCIT-2xPH$^{PLC\delta1}$ was occasionally observed (Figures 8A and 8B), as indicated by a previous study (Shimada et al., 2019). This result is in contrast to the absence of mCIT-2xPH^{FAPP1}

Figure 6. (continued).

(D) Callose deposition. *Ec*-inoculated leaves were fixed and stained by both aniline blue and Alexa Fluor 488-conjugated wheat germ agglutinin (WGA). The images were obtained by merging the confocal optical sections (Z-stacks).

(E) H_2O_2 production. *Ec*-inoculated fresh leaves were stained by 3,3'-diaminobenzidine, fixed, and viewed by compound microscopy. H_2O_2 accumulation is indicated by brownish color.

(F) Accumulation of autofluorescence materials. *Ec*-inoculated leaves were fixed, and the autofluorescence was directly viewed by fluorescence microscopy.

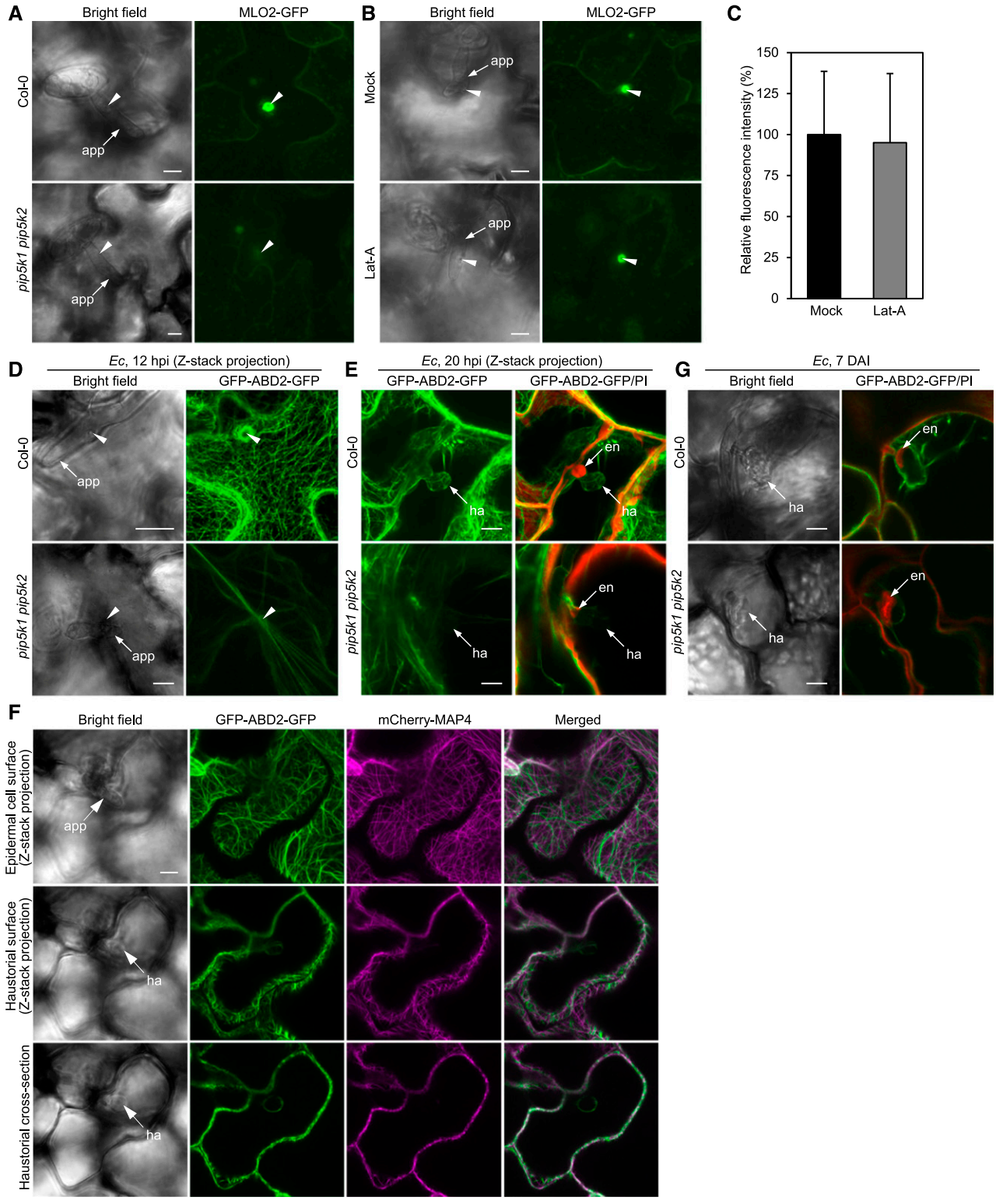

Figure 7. Impaired Cellular Responses Associated with Host Susceptibility to Powdery Mildew Infection in the *pip5k1 pip5k2* Mutant.

(A) Recruitment of MLO2-GFP into *Ec* penetration sites is impaired in *pip5k1 pip5k2*. Leaves of Col-0 and *pip5k1 pip5k2* plants expressing MLO2:MLO2-GFP at 13 hpi were examined by confocal microscopy. The images were obtained by merging the confocal optical sections (Z-stacks).

at the EHM surrounding the powdery mildew and white rust haustoria (Figure 1; Supplemental Figure 3), suggesting that the EHM encompassing haustoria and the EIHM surrounding *Ch* primary hyphae are not one homogenous entity but instead are composed of distinct phosphoinositide pools. Nevertheless, PI(4,5)P_2 appears as a conserved and predominant phosphoinositide of both membrane compartments.

To evaluate the susceptibility of the *pip5k1 pip5k2* mutant to *Ch*, intact plants of the wild type and the *pip5k1 pip5k2* mutant were sprayed with conidia of *Ch*. At 3 DAI, wild-type leaves showed water-soaking lesions, and infected plants subsequently became withered and eventually died at 4 DAI. In contrast, *pip5k1 pip5k2* plants barely produced visible anthracnose symptoms (Figure 8C). Likewise, droplet inoculation on detached leaves further revealed that necrotic water-soaked lesions surrounded by chlorotic halos developed at the inoculation sites of wild-type leaves at 3 DAI, and water-soaked lesion expansion and tissue maceration rapidly spread over the inoculated leaf. The infection on leaves of *pip5k1 pip5k2* plants was strictly restricted at the inoculated site and did not spread beyond the inoculated area at extended incubation time until 6 DAI (Supplemental Figure 12). Thus, PI(4,5)P_2, the resulting product of PIP5K1 and PIP5k2, is an important determinant factor of host susceptibility to the hemibiotrophic *Colletotrichum* fungus as well as to the haustorium-forming biotrophic powdery mildew and white rust pathogens.

To investigate which stage of fungal development was impaired in the *pip5k1 pip5k2* mutant, we collected leaf tissues of wild-type and *pip5k1 pip5k2* plants inoculated with *Ch* for microscopic examination. At 2 DAI, large primary hyphae colonized leaf epidermal cells of wild-type and *pip5k1 pip5k2* plants (Figure 8D). In infected cells of wild-type plants at 3 DAI, abundant thin secondary hyphae arose from primary hyphae and spread into several adjacent cells in leaf tissues showing water-soaking lesions. At 4 DAI, leaf tissues of the wild type completely collapsed, with systemic colonization by fungal secondary hyphae (Figure 8D). In contrast, in epidermal cells of *pip5k1 pip5k2* plants until 4 DAI, most infection sites were associated with extensive growth of primary hyphae, resulting in the first infected cells becoming filled with fungal hyphae.

To test whether extensive growth of primary hyphae within infected leaf epidermal cells of *pip5k1 pip5k2* plants at 4 DAI was still associated with the biotrophic phase of the interaction, infected leaf tissues were submitted for plasmolysis to assess the viability of host cells. Epidermal cells of *pip5k1 pip5k2* plants with extensive colonization of primary hyphae as well as adjacent noninfected cells displayed plasmolysis, and intact tonoplast membrane was clearly visible within the plasmolyzed cytoplasm of the infected cell (Figures 8E and 8F; Supplemental Movie 5). These results suggest that PI(4,5)P_2 is present at the biotrophic interface in the *Ch*-Arabidopsis interaction, and mutation of both *PIP5K1* and *PIP5K2* genes inhibits the transition from the biotrophic to the necrotrophic stage, thus preventing the development of visible necrotic symptoms.

DISCUSSION

The structural singularity of the EHM has been well documented for the haustoria formed by powdery mildew and rust fungi. This membrane is continuous with the plant PM (Littlefield and Bracker, 1970), but the properties and molecular composition of the EHM are distinct. Electron micrographs reveal that an electron-dense haustorial neckband appears at the junction of the host PM, and the EHM exhibits a thick and convoluted appearance, which is distinct from the thin, smooth host PM (Gil and Gay, 1977; Celio et al., 2004; Micali et al., 2011). Furthermore, the EHM appears to lack several common plant PM proteins (Spencer-Phillips and Gay, 1981; Koh et al., 2005; Micali et al., 2011), instead possessing a unique set of membrane proteins of the endomembrane system (Inada et al., 2016; Berkey et al., 2017; Kwaaitaal et al., 2017). In this study, we show that the host PM and EHM differ in their constituent lipids: both PI4P and PI(4,5)P_2 localize at the PM, although PI(4,5)P_2 is found in relatively low abundance in plant cells (van Leeuwen et al., 2007; Vermeer et al., 2009; Munnik and Vermeer, 2010; Munnik and Nielsen, 2011; Simon et al., 2014, 2016), whereas only PI(4,5)P_2, but not PI4P, is integrated into the EHM of powdery mildew (Figure 1). This distinct distribution pattern also appears on the EHM among other haustorium-forming biotrophs, such as the white rust *A. candida* (Supplemental Figure 3) and the downy mildew *Hyaloperonospora arabidopsidis* (Shimada et al., 2019). In contrast, both PI(4,5)P_2 and PI4P are present at the EIHM enclosing the invasive hyphae of hemibiotroph *Ch* (Figure 8; Shimada et al., 2019) and at the

Figure 7. (continued).

(B) and **(C)** Focal aggregation of MLO2-GFP at *Ec* penetration sites is regulated via an actin-independent mechanism. Leaves of Col-0 plants expressing MLO2:MLO2-GFP were infiltrated with water (Mock) or 5 μM latrunculin A (Lat-A) and subsequently inoculated with *Ec*. At 13 hpi, the infected epidermal cells were examined by confocal microscopy.

(B) Representative images obtained by merging the confocal optical sections (Z-stacks).

(C) Relative fluorescence intensity of MLO2-GFP around penetration sites. Quantification was performed over 30 sites per treatment. Data are means ± SD ($n = 30$). P = 0.665, Student's *t* test.

(D) to **(G)** Dynamics of AFs at the *Ec* penetration sites and on the peripheral surface of haustoria in leaf tissues of Col-0 and *pip5k1 pip5k2* plants expressing GFP-ABD2-GFP.

(D) Spatial organization of AFs underneath the *Ec* penetration sites at 12 hpi.

(E) Spatial organization of AFs on the haustorial surface during haustorial development at 20 hpi.

(F) AFs but not microtubules dynamically reorganized on the haustorial surface. Leaves of Col-0 plants simultaneously expressing GFP-ABD2-GFP and mCherry-MAP4 at 20 hpi were examined by confocal microscopy. The same inoculation sites are viewed on the peripheral surface of leaf epidermis (top row; Z-stacks), on the haustorial surface (middle row; Z-stacks), or on the haustorial cross section (bottom row; single section).

(G) Dynamic responses of AFs associated with mature haustoria at 7 DAI.

Arrowheads indicate the *Ec* penetration site. app, appressorium; en, encasement; ha, haustorium. Bars = 10 μm.

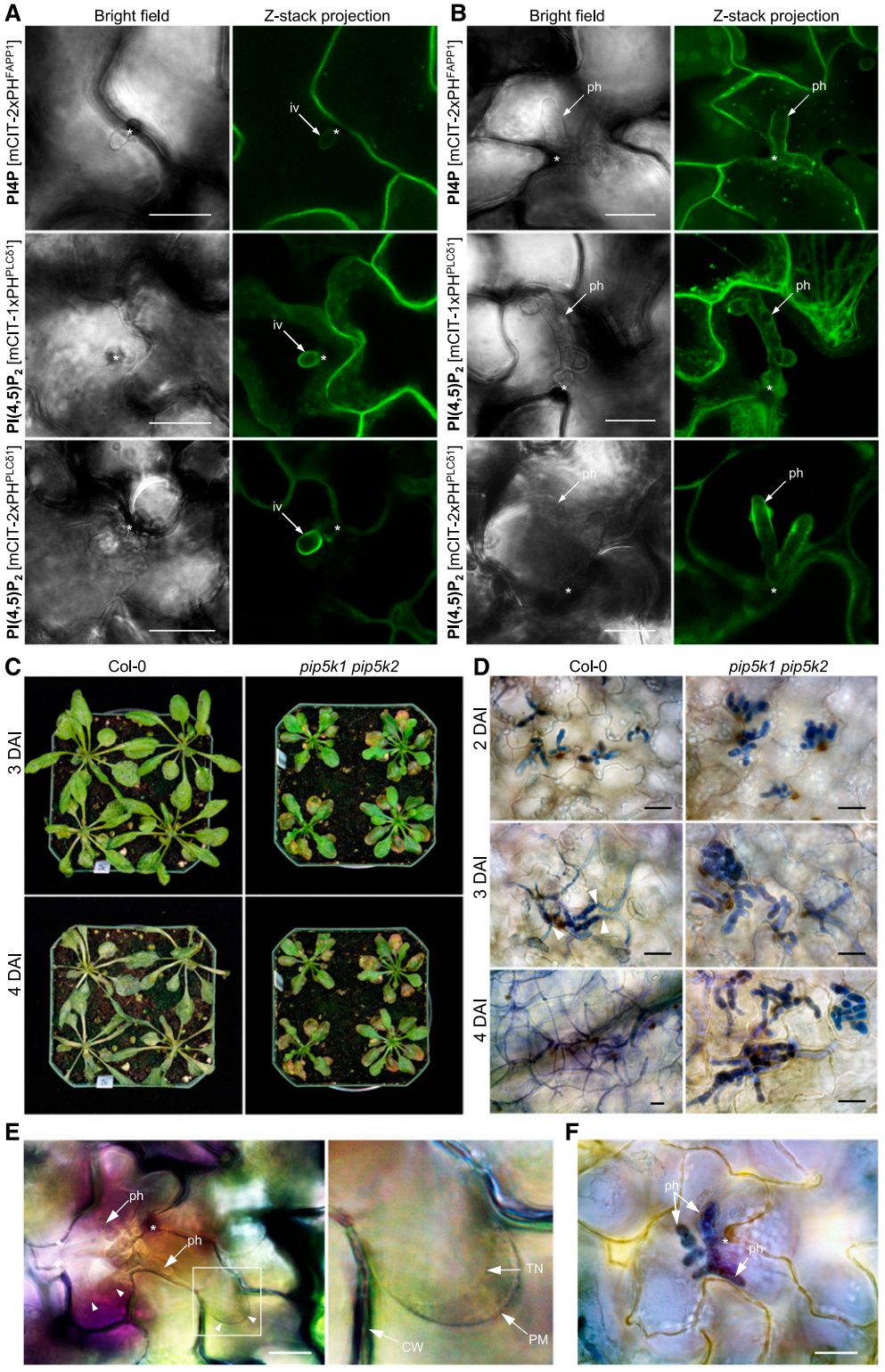

Figure 8. Regulation of PI(4,5)P_2 Controls Disease Development in Plants and the Lifestyle of the Hemibiotrophic Fungal Pathogen *Ch*.

(A) and **(B)** Association of the PI4P biosensor mCIT-2xPH^{FAPP1} and the PI(4,5)P_2 biosensors mCIT-1xPH$^{PLC\delta1}$ and mCIT-2xPH$^{PLC\delta1}$ with the biotrophic stages of the *Ch* life cycle. Both PI4P and PI(4,5)P_2 signals targeted the surface of infection vesicles (iv; **[A]**) and primary hyphae (ph; **[B]**). Asterisks indicate the penetration sites.

periarbuscular membrane formed during arbuscular mycorrhizal symbiosis (Ivanov and Harrison, 2019). The distinct nature of the EHM from the EIHM and periarbuscular membrane led us to explore the impact of PI4P absence on the characteristics of the EHM and the potential role of PI(4,5)P_2 on the functionality of haustoria.

In mammalian cells, PI4P is generated in many cellular membranes, including a major pool in the Golgi/*trans*-Golgi network and two relatively minor pools at the PM and late endosomes/lysosomes (Hammond et al., 2014). PI4P enriched at the cytosolic face of the *trans*-Golgi in mammalian cells recruits cytosolic proteins that bind to PI4P and functions in Golgi-to-PM trafficking (Lenoir and Overduin, 2013; Makowski et al., 2017). In contrast, PI4P in plant cells predominantly accumulates at the PM, establishing it as a hallmark of this membrane (Simon et al., 2014, 2016). Critical roles of PI4P at the PM in animal and plant cells were only recently recognized, as PI4P generates a high electrostatic field that contributes to the PM localization and function of proteins with polybasic motifs, including proteins involved in cytoskeleton dynamics, hormone transport, and receptor-like kinase signaling (Hammond et al., 2012; Simon et al., 2014, 2016). Additionally, recent data indicate that multiple PI4P binding proteins function as nonvesicular lipid transporters and drive lipid export from the endoplasmic reticulum to other organelles through the reciprocal transfer of PI4P at membrane contact sites (Cockcroft and Raghu, 2018). Thus, PI4P together with its effector proteins play essential roles in membrane biogenesis, cell signaling, and cellular trafficking. The lack of PI4P at the EHM likely contributes to the inability to anchor effector proteins at the EHM and further neglects the impact of a PI4P-driven physical membrane property at the EHM.

Using PI4P as the precursor, PIP5Ks participate in the biosynthesis of PI(4,5)P_2, which primarily takes place at the PM (Simon et al., 2014). Notably, both PIP5K1 and PIP5K2 are ubiquitously expressed in Arabidopsis and locate at the PM (Ischebeck et al., 2013), but they are absent from the EHM (Supplemental Figure 9). The absence of PIP5Ks and their precursor PI4P at the EHM suggests that PIP5K1 and PIP5K2 are not directly involved in the in situ synthesis of PI(4,5)P_2 at the EHM, and the PI(4,5)P_2 pool at the EHM is likely derived from the PM. We observed that PI(4,5)P_2 signals likely bundled to the cytoskeleton between the host PM and the EHM (Supplemental Figure 1C). Disruption of actin filaments by latrunculin A prevents the trafficking of PI(4,5)P_2, resulting in a weak signal intensity of PI(4,5)P_2 on the EHM (Figures 3A and 3B), indicating that the transport of PI(4,5)P_2 to the surface of the EHM is mediated by the actin cytoskeleton. Intriguingly, targeting of PI(4,5)P_2 signals to the EHM is not inhibited by BFA, a fungal toxin that inhibits the activity of ARF-GEF GNOM-mediated vesicular trafficking in both endocytic and secretory pathways. This result supports the targeting of PI(4,5)P_2 to the EHM independent from the GNOM-mediated vesicular transport. Whether other BFA-insensitive ARF-GEFs, such as BIG3 and/or BIG5/MIN7 (Geldner et al., 2003; Nomura et al., 2011; Richter et al., 2014), mediate the transport of PI(4,5)P_2 to the EHM remains to be determined. In eukaryotic cells, PI(4,5)P_2 is concentrated in sterol-rich domains at the PM (Pike and Miller, 1998; Graber et al., 2014; Stanislas et al., 2015). Upon depletion of phytosterols in Arabidopsis leaves by MβCD treatment, PI(4,5)P_2 signals are significantly reduced at the EHM as well as at the PM (Figures 3A and 3B), suggesting that the steady level of cellular sterols is required to maintain PI(4,5)P_2 pools at the PM and the EHM. Taken together, our data suggest that during the establishment of powdery mildew haustoria, PI(4,5)P_2 at the EHM is likely derived from the PI(4,5)P_2 pool synthesized from PI4P at the PM, and the lateral transport of PI(4,5)P_2 from the PM to the EHM is actin-dependent.

Cellular imaging of PI(4,5)P_2 biosensors provides an indirect way to localize this phospholipid. The biosensor $PH^{PLC\delta1}$ has a high selectivity for PI(4,5)P_2 and has been robustly expressed in many different organisms, including yeast, mammalian, and plant cells, where the $PH^{PLC\delta1}$ biosensor is recruited to the membranes that accumulate this lipid (Platre and Jaillais, 2016). Notably, under low levels or in the absence of target lipid, the biosensor $PH^{PLC\delta1}$ remains unbound in the cytosol, making it unsuitable to quantitatively measure PI(4,5)P_2 contents with spatial resolution (van Leeuwen et al., 2007; Platre and Jaillais, 2016). Nonetheless, increased signal intensity of the $PH^{PLC\delta1}$ biosensor was observed at the PM under conditions known to induce PI(4,5)P_2 synthesis or prevent its hydrolysis, such as high NaCl concentration or inhibition of phosphoinositide-specific PLC activity (van Leeuwen et al., 2007; Lee et al., 2019). Thus, a positive correlation exists between the signal intensity of the $PH^{PLC\delta1}$ biosensor and the PI(4,5)P_2 contents under conditions where this lipid becomes concentrated in membranes (van Leeuwen et al., 2007; Lee et al., 2019; Colin and Jaillais, 2020). Upon powdery mildew infection, the fluorescence intensity of the PI(4,5)P_2 biosensor mCIT-1x$PH^{PLC\delta1}$ is specifically elevated in the infected cells, suggesting increased PI(4,5)P_2 levels in host cells during the infection process. Increased PI(4,5)P_2 content appears to be tightly associated with the host PM dynamics and is focally aggregated around the pathogen penetration site and integrates into the EHM. Active recruitment of PI(4,5)P_2 into interaction sites suggests that pathogen infection alters the distribution of PI(4,5)P_2 to modulate

Figure 8. (continued).

(C) Disease development on Col-0 and *pip5k1 pip5k2* plants. *Ch*-inoculated plants were photographed at 3 and 4 DAI.

(D) Microscopic images of *Ch*-infected leaf tissues. In *pip5k1 pip5k2* leaves, extensive bulbous primary hyphae were restricted within the first infected epidermal cells during the infection time course 2 to 4 DAI, whereas in Col-0 plants, thin necrotrophic hyphae developed at 3 DAI and rapidly spread into neighboring cells. Infected leaf tissues were stained with trypan blue.

(E) and **(F)** Extended biotrophic stages of *Ch* infection in the *pip5k1 pip5k2* mutant.

(E) Viability of *Ch*-infected cells at 4 DAI is shown by the host protoplasm contracting from the cell wall (CW) after plasmolysis. The right panel shows an enlarged view of the boxed area in which tonoplast (TN) is clearly distinguishable from the PM.

(F) Leaf sample showing that the same *Ec*-infected site in **(E)** was fixed and stained for fungal hyphae with trypan blue.

Bars = 20 μm.

the cellular activities of host cells. Although $PI(4,5)P_2$ is a minor component of the PM, its functions are broad (Tan et al., 2015). $PI(4,5)P_2$ is able to directly recruit and/or activate integral and peripheral membrane proteins that function in several essential cellular processes, including the regulation of cellular trafficking, actin polymerization, focal adhesion assembly, and polarity establishment (Tan et al., 2015; Noack and Jaillais, 2017). Over the last decade, $PI(4,5)P_2$ has been shown to play physiological roles in plants in the regulation of auxin transport (Mei et al., 2012; Ischebeck et al., 2013), stomatal opening (Lee et al., 2007), root hair development (Kusano et al., 2008; Stenzel et al., 2008), pollen tube growth (Ischebeck et al., 2008, 2010, 2011; Sousa et al., 2008; Gillaspy, 2013), and biotic and abiotic stress responses (Williams et al., 2005; Munnik and Vermeer, 2010; Shimada et al., 2019). Many of these processes occur in a strict spatially and temporally regulated fashion, requiring precise $PI(4,5)P_2$ targeting and concentrations (Krishnamoorthy et al., 2014; Noack and Jaillais, 2017). In this study, we showed that inactivation of Arabidopsis PIP5K activity, caused by *PIP5K1* and *PIP5K2* gene knockouts, results in the depletion of PM $PI(4,5)P_2$ and diminishes the assembly and organization of cortical AFs. In support of these findings, $PI(4,5)P_2$ is the best-characterized regulator of actin cytoskeleton in yeast and mammalian cells among the functionally characterized phosphoinositides. $PI(4,5)P_2$ interacts directly with several central actin binding proteins such as profilin, cofilin/ADF, formins, N-WASP, and capping proteins as well as many signaling and scaffolding proteins, which interact with actin binding proteins to control their activities and/or subcellular localization. As a consequence, $PI(4,5)P_2$ promotes the formation of AF structures adjacent to the inner leaflet of the PM (Saarikangas et al., 2010; Senju and Lappalainen, 2019). Although the actin cytoskeleton and its accessory elements are highly conserved across eukaryotic species, the regulation of actin binding proteins and associated proteins by $PI(4,5)P_2$ has yet to be validated in plants.

Upon powdery mildew infection of the *pip5k1 pip5k2* mutant, $PI(4,5)P_2$ depletion results in a concomitant reduction in the organization and dynamics of AFs under the pathogen penetration site and surrounding the haustorial surface. The actin cytoskeleton of host cells is commonly harnessed by intracellular pathogens to promote their own survival, replication, and cell-to-cell spread in various animal systems (Galán and Collmer, 1999; Galán and Zhou, 2000; Gouin et al., 2005). The diminished AF assembly and dynamics observed in the *pip5k1 pip5k2* mutant at powdery mildew fungus interaction sites is likely to facilitate actin-dependent cellular processes required for powdery mildew disease development. For instance, AF arrangement on the haustorial surface was observed in the barley-powdery mildew system (Opalski et al., 2005) and was suggested to guide the spatial shaping of haustoria and/or deliver the molecules needed by the pathogen to feeding structures (Schmidt and Panstruga, 2007). The *pip5k1 pip5k2* mutant is also defective for focal accumulation of MLO2-GFP at the pathogen's attempted penetration sites and displays an enhanced penetration resistance against powdery mildew. The role of *MLO* genes as a major susceptibility factor to powdery mildews has been demonstrated in a wide range of monocot and dicot species (Kusch and Panstruga, 2017). Polarized MLO accumulation at pathogen penetration sites appears to be independent of actin cytoskeleton functions (Figure 7; Bhat et al., 2005; Feechan et al., 2013) and potentially modulates focal actin reorganization at the penetration site (Opalski et al., 2005). However, the function of *mlo* in penetration resistance at the cell periphery requires both actin-dependent and actin-independent pathways (Opalski et al., 2005; Miklis et al., 2007). Therefore, PM $PI(4,5)P_2$ may also regulate the actin cytoskeleton-independent cellular trafficking that is required for MLO localization during powdery mildew infection. While the effects of cellular $PI(4,5)P_2$ depletion in the *pip5k1 pip5k2* mutant on AF dynamics and focal MLO accumulation during powdery mildew infection are clear, the underlying mechanisms remain unknown. Targeted depletion of $PI(4,5)P_2$ specifically at the EHM could provide a specific strategy to evaluate the impact of $PI(4,5)P_2$ on haustorial formation and function. Given that $PI(4,5)P_2$ has pleiotropic effects in regulating cellular functions, future work should address whether $PI(4,5)P_2$ depletion contributes to enhanced disease resistance in *pip5k* mutants through other cellular processes.

The depletion of $PI(4,5)P_2$ in the *pip5k1 pip5k2* mutant results in reduced disease incidence by inhibiting multiple stages of pathogen development of biotrophic powdery mildew, white rust, and the hemibiotrophic *Colletotrichum* pathogens. On *pip5k1 pip5k2* leaves, powdery mildew establishment displays a low penetration rate, decreased haustorial development, and poor hypha growth. Likewise, restricted symptom development in *pip5k1 pip5k2* mutants is associated with the prevention of the switch from a biotrophic to a necrotrophic lifestyle of hemibiotrophic *Ch*. Evidently, no cell death was detected at either powdery mildew or *Ch* infection sites on *pip5k1 pip5k2* plants. Moreover, upon powdery mildew inoculation, *pip5k1 pip5k2* mutants show similar levels of accumulation of autofluorescent compounds, callose deposition, and H_2O_2 production at infection sites as compared with the wild type. These results indicate that these cellular defense activities have a negligible contribution to enhanced disease resistance in the *pip5k1 pip5k2* mutant. However, the expression of several defense-responsive genes, including *PR1*, *PR2*, *BG3*, and *PR4*, is significantly greater in the *pip5k1 pip5k2* mutant as compared with the wild type upon powdery mildew infection. Intriguingly, the expression of these defense-associated genes is induced in an SA-independent manner, since many genes involved in SA synthesis and signaling are downregulated in the mutant compared with the wild type (Figure 5A). In addition, we found that the SA level in the *pip5k1 pip5k2* mutant is reduced to 55% of the wild-type levels. A previous study indicated that sustained activation of two mitogen-activated protein kinases, MPK3 and MPK6, could be sufficient to confer SA-independent regulation of most SA-responsive genes in Arabidopsis (Tsuda et al., 2013). Recent work showed that phosphorylation by MPK6 inhibits PIP5K6 activity and controls $PI(4,5)P_2$ production in the apical PM domain for tip growth of pollen tubes (Hempel et al., 2017). It would be interesting to examine whether MAPK activation is similarly involved in regulating SA-responsive genes in the *pip5k1 pip5k2* mutant.

In conclusion, our results demonstrate that the inhibition of multiple stages of disease progression in the *pip5k1 pip5k2* mutant does not involve the enhanced activation of cellular defenses and cell death associated with cell wall lignification, callose deposition, and reactive oxygen species accumulation. We further show that reduced disease incidence of powdery mildew and

Colletotrichum anthracnose appears to be the result of impaired susceptibility of the mutant.

METHODS

Plant Materials and Growth Conditions

Arabidopsis (*Arabidopsis thaliana*) plants were grown at 21°C with a 16-h photoperiod of ~125 μE m^{-2} s^{-1}. All single T-DNA insertion mutants, *pip5k1* (SALK_146728, At1g21980), *pip5k2* (SALK_012487, At1g77740; Ischebeck et al., 2013), *pip5k5* (SALK_147475, At2g41210), *pip5k7-1* (SALK_151429, At1g10900), *pip5k8* (SAIL_561_F09, At1g60890), and *pip5k9* (WiscDsLox434B6, At3g09920), were acquired from the ABRC. The double mutant *pip5k1 pip5k2* was generated by crossing single mutants and propagated from the offspring of self-crossed plants *pip5k1*$^{+/-}$/*pip5k2*$^{-/-}$, since the homozygous double mutant did not produce flowers. The homozygosity of all T-DNA mutants was genotyped by PCR with both gene-specific and T-DNA border primers listed in Supplemental Table 2.

Arabidopsis transgenic lines tagged with fluorescent proteins used in this study are as follows: 35S:GFP-LTI6b (Cutler et al., 2000), 35S:PMA-GFP (Lefebvre et al., 2004), 35S:GFP-ABD2-GFP (Wang et al., 2008), mCherry-MAP4 (El Zawily et al., 2014), ER-GFP (CS16251), Tono-CFP (CS16256), and Tono-GFP (CS16257; Nelson et al., 2007), Cyto-YFP (CS68117; DeBono et al., 2009), pUBQ10:YFP (CS781646; Geldner et al., 2009), RPW8.2:RPW8.2-YFP and RPW8.2:RPW8.2-RFP (Wang et al., 2007), MLO2:MLO2-YFP (Jones et al., 2017), and PIP biosensors pUBQ10:mCIT-1xPH$^{PLC\delta1}$ (P14Y), pUBQ10:mCIT-2xPH$^{PLC\delta1}$ (P24Y), pUBQ10:mCIT-1xTUBBY-C (P15Y), pUBQ10:mCIT-2xPH^{FAPP1} (P21Y), pUBQ10:mCIT-1xPH^{FAPP1} (P5Y), pUBQ10:2xCyPet-1xPH^{FAPP1} (P5C), pUBQ10:mCIT-P4M^{SiDM} (P4M), and pUBQ10:mCIT-2xFYVE^{HRS} (P18Y; Simon et al., 2014, 2016).

Constructs and Plant Transformation

To create a construct expressing PIP5K1-YFP, a DNA fragment containing an ~3.5-kb open reading frame of the *PIP5K1* gene and an ~2.1-kb promoter region was amplified from the Arabidopsis genomic DNA with primers *Spe*I-PIP5K1-FP and *Kpn*I-PIP5K1-RP (Supplemental Table 2). After digestion with enzymes *Spe*I and *Kpn*I, the fragment was ligated into binary backbone vector pCNYHB (Yang et al., 2018), generating pPIP5K1:PIP5K1-YFP. To produce a construct expressing PIP5K2-YFP, a DNA fragment containing an ~3.3-kb open reading frame of the *PIP5K2* gene and an ~2.2-kb promoter region was amplified from the genomic DNA with primers *Xba*I-PIP5K2-FP and *Sma*I-PIP5K2-RP (Supplemental Table 2). After digestion with enzymes *Xba*I and *Sma*I, the fragment was ligated into pCNYHB, generating pPIP5K2:PIP5K2-YFP. The plasmids were introduced into *Agrobacterium tumefaciens* strain EHA105 and then transformed into Col-0 plants using floral dipping (Zhang et al., 2006). T1 seeds were selected on Murashige and Skoog medium with kanamycin.

Pathogen Inoculation

The Arabidopsis-adapted powdery mildew fungus *Erysiphe cichoracearum* (Liu et al., 2010) was maintained and propagated on host cucumber (*Cucumis sativus*, variety Sweet Slice; McKenzie) plants. Three- to 4-week-old Arabidopsis plants were inoculated with conidiospores at a density of 5 to 10 conidia mm^{-2}. Inoculated leaves at the indicated time points post inoculation were detached, fixed, and stained as previously described (Yang et al., 2014).

The adapted anthracnose pathogen *Colletotrichum higginsianum* on Arabidopsis was propagated and handled as described previously (Liu et al., 2007b). For disease assays, 3- to 4-week-old Arabidopsis plants were sprayed with conidial suspensions or spotted with droplets (1×10^6 conidiospores mL^{-1} in distilled water), and immediately the inoculated plants were placed into a 100% humidity chamber. Inoculated plants were photographed following the infection time course, and infected leaves, at different time points post inoculation, were detached, fixed, and stained in trypan blue (Liu et al., 2007b).

Maintenance and inoculation of the white rust *Albugo candida* isolate Acem1 on host Arabidopsis were performed using the described methods (Borhan et al., 2001). Briefly, *A. candida* was maintained on Arabidopsis *NahG* plants. Zoosporangia were scratched off the *A. candida*-colonized leaf surface, resuspended in water (10^5 mL^{-1}), and incubated on ice for 30 min for zoospore release. The plants were inoculated by placing a drop of inoculum (10 μL) on each leaf and grown under a closed incubation chamber to retain humidity. The inoculated plants were placed in a cold incubator (14 to 16°C) in the dark overnight and then kept under a 10-h-light/14-h-dark cycle for disease development.

Chemical Treatments

The following stock solutions in DMSO were used: 1 mM latrunculin A (Sigma-Aldrich), 50 mM BFA (Sigma-Aldrich), 100 mM oryzalin (Sigma-Aldrich), 20 mM wortmannin (Sigma-Aldrich), and 10 mM FM4-64 (Thermo Fisher Scientific). Stocks were stored at −20°C and subsequently diluted in water to the specified concentrations for experiments. The following working concentrations were used: 5 μM latrunculin A, 1 mM oryzalin, 300 μM BFA, 1 mM MβCD, 30 μM wortmannin, and 50 μM FM4-64. Leaves of Arabidopsis were preinfiltrated with latrunculin A, oryzalin, BFA, MβCD, or wortmannin working solutions. After 1 h of incubation, infiltrated leaves were inoculated with *Ec* conidiospores. At 24 hpi, inoculated leaves were examined with a confocal microscope. For plasmolysis experiments, leaves were mounted in 0.85 M KCl and incubated for 15 min before imaging.

Microscopy and Imaging

Inoculated and noninoculated leaves were harvested at varying time points, and fresh or fixed leaf tissues were examined by microscopy. The leaves were fixed in fixing buffer (60% [v/v] methanol, 30% [v/v] chloroform, and 10% [v/v] acetic acid). After rehydration through an ethanol gradient, leaves were stained with 0.05% (w/v) trypan blue, 0.05% (w/v) aniline blue, and/or 10 μM Alexa Fluor488 conjugate of wheat germ agglutinin (Life Technologies) as the experiment required, followed by light microscopy (AxioPlan, Zeiss) or confocal laser scanning microscopy (Zeiss LSM 510 Meta). Aniline blue was used to detect callose in 150 mM K_2HPO_4 (pH 9.5) or to stain fungal hyphae in acidic water. Macroscopic detection of H_2O_2 accumulation by 3,3'-diaminobenzidine staining was performed as described earlier (Liu et al., 2007a). Fresh leaves were incubated in either distilled water or 10 μM propidium iodide (PI; Life Technologies), followed by confocal microscopy. The fluorescence was detected using a confocal microscope with the following settings of excitation/emission wavelengths: CFP and callose (405/420 to 480 nm), GFP (488/505 to 530 nm), RFP (543/581 to 635 nm), YFP (514/530 to 560 nm), PI (488/>560 nm), and FM4-64 (488/>650 nm). Images were analyzed and made with software LSM Image Browser, Adobe Photoshop, or ImageJ.

Quantification of YFP signal intensity was performed by confocal microscopy acquired under strictly identical acquisition parameters (laser power, pinhole, detector gains, speed, zoom factor, resolution, and so on). Intensity quantification was performed using ImageJ. Average intensity was measured and corrected to the average background signal. Quantification was performed over three plants for each genotype ($n = 30$).

Immunofluorescence

Fully expanded rosette leaves were excised from 4-week-old Arabidopsis plants, and the abaxial surface was inoculated with *Ec* conidiospores at

a density of 5 to 10 conidia mm^{-2}. Inoculated leaves were incubated in humid Petri dishes at 21°C for 36 hpi. The adaxial epidermal leaf surface was affixed to Scotch transparent adhesive tape with the abaxial side facing upward. Subsequently, another strip of the tape was firmly topped on the abaxial surface of the affixed leaf. The upper tape was then gently pulled away from the lower tape, peeling away the abaxial epidermal cell layer attached to the lower tape. Epidermal peels attached on the transparent tapes were cut to ~3 × 5 mm and fixed with 4% methanol-free formaldehyde and 0.2% glutaraldehyde in 0.1 M PBS (pH 7.0) at 4°C overnight.

Monoclonal anti-PI(4,5)P_2 antibody (clone 2C11, Z-P045) and anti-PI4P antibody (Z-P004) were purchased from Echelon Biosciences. Immunofluorescence studies were performed following the protocol described by Hammond at al. (2009) with some modifications. All steps from fixation to antibody incubation were performed on ice or at 4°C. After fixation, the epidermal peels were rinsed three times with PBS and digested by incubation with cell wall-degrading enzyme mix (0.05% cellulase and 0.1% pectinase in PBS, pH 5.0) for 30 min. Then epidermal peels were blocked and permeabilized for 40 min of incubation with a solution containing 5% (w/v) skim milk and 0.5% (w/v) saponin (Quillaja bark; Sigma-Aldrich). The epidermal peels were incubated with primary anti-PI(4,5)P_2 (1:200) or anti-PI4P (1:200) antibody at 4°C overnight, followed by incubation with the secondary antibody Alexa Fluor 488 goat anti-mouse IgG (1:200; Abcam) for 4 h. The epidermal peels were mounted in ProLong Gold antifade reagent (Invitrogen) and examined with a Zeiss 880 confocal microscope.

RNA-Seq and RT-PCR Analysis

Three- to 4-week-old Arabidopsis Col-0 wild-type and *pip5k1 pip5k2* plants were inoculated with *Ec* conidiospores. The leaves without or with *Ec* inoculation at 2, 5, and 7 DAI were collected, flash-frozen in liquid nitrogen, and stored at −80°C until required. Three biological replicates were obtained for each sample. RNA samples were prepared using the Plant RNA Isolation Mini Kit (Agilent Technologies) according to the manufacturer's protocol. The yield and purity of RNA were determined with Nanodrop 1100 (Thermo Fisher Scientific), and the quality was verified using an Agilent 2100 Bioanalyzer (Agilent Technologies). Purified total RNA was precipitated and resuspended in RNase-free water to a final concentration of 100 ng μL^{-1}. A total of 36 cDNA libraries were constructed using the TruSeq RNA Sample Preparation Kit (Illumina). Paired-end sequencing was conducted on the Illumina HiSeq2500 Sequencing System, generating 101-nucleotide reads at the National Research Council, Aquatic and Crop Resource Development, in Saskatoon, Canada. Sequencing adapters were removed, and low-quality reads were trimmed using Trimmomatic with default settings (Bolger et al., 2014). Reads were mapped to the annotated Arabidopsis genomes (The Arabidopsis Information Resource 10) using STAR (Dobin et al., 2013). Transcripts were identified using StringTie (Pertea et al., 2015) followed by the Cuffmerge tool (Trapnell et al., 2012). HTseq-count (Anders et al., 2015) was used to count the reads spread across the exonic regions of each gene. Differential expression analysis was performed with DESeq2 between mutants and the wild type (Love et al., 2014). Normalized read counts from DESeq2 were expressed as gene expression levels. Genes with less than 10 reads across all samples were excluded to eliminate the extremely low expressed transcripts. Differential gene expression analysis was performed with DESeq2 between mutants and the wild type at 2, 5, and 7 DAI. To identify genes with significant expression differences, a cutoff of false discovery rate < 0.01 and $\log_2$ fold change ≥ 1 was applied. The heat map was generated with the R pheatmap package.

For RT-PCR analysis, cDNA was synthesized from 1 μg of total RNA using the QuantiTect Reverse Transcription kit (Qiagen). Gene expression levels were evaluated by RT-PCR for 25 or 28 cycles. The gene *eIF4A1* was used as an internal control to normalize the amount of cDNA template. Primers used in this study are listed in Supplemental Table 2.

Hormone Measurement

Four-week-old Arabidopsis Col-0 and *pip5k1 pip5k2* plants were inoculated with *Ec* conidiospores at a density of 5 to 10 conidia mm^{-2} or with mock. Leaves at 5 DAI were harvested and immediately frozen in liquid nitrogen for SA and JA analyses. Three biological replicates were obtained for each sample. The extraction and quantification of SA and JA were performed according to the method previously by Liu et al. (2010).

Statistical Analysis

Two-tailed Student's *t* test was used for paired comparison of the fluorescence intensities or fungal development between treatments versus mock or the wild type versus the mutant (*, $P < 0.05$; **, $P < 0.01$; and ***, $P < 0.001$). One-way ANOVA with Tukey's HSD test was performed for multiple comparisons. Samples with statistically significant differences are marked with different letters ($P < 0.05$, lowercase letters; $P < 0.01$, uppercase letters). Error bars in all figures represent SD. The number of replicates is reported in the figure legends. All statistical analyses with ANOVA and/or Student's *t* test are included in Supplemental Data Set 2.

Accession Numbers

Sequence data from this article can be found in the Arabidopsis Genome Initiative or GenBank/EMBL databases under the following accession numbers: PIP5K1 (At1g21980), PIP5K2 (At1g77740), PIP5K5 (At2g41210), PIP5K7 (At1g10900), PIP5K8 (At1g60890), PIP5K9 (At3g09920), MLO2 (At1g11310), RPW8.2 (AF273059), PR1 (At2g14610), PDF1.2a (At5g44420), FRK1 (At2g19190), and eIF4A1 (At3g13920). The RNA-seq data used in this study are available in the Gene Expression Omnibus database under accession number GSE127919.

Supplemental Data

Supplemental Figure 1. Spatial distribution of PI4P and PI(4,5)P_2 at penetration sites of the powdery mildew *E. cichoracearum*.

Supplemental Figure 2. Differential distribution of host cellular membrane compartments in association with the haustorium of the powdery mildew *E. cichoracearum*.

Supplemental Figure 3. Differential distribution of phosphoinositides to the haustorial periphery of *Albugo candida*.

Supplemental Figure 4. Increased production of PI(4,5)P2 in *Ec*-colonized leaf epidermal cells.

Supplemental Figure 5. Expression profiling of Arabidopsis PI4P 5-kinase genes and characterization of T-DNA insertion mutants.

Supplemental Figure 6. Growth phenotypes of the Arabidopsis knockout mutants and complemented mutant plants of PI4P 5-kinase genes.

Supplemental Figure 7. Pathogenicity assays on Col-0 and *pip5k* double, triple and quadruple mutant plants against the white rust *Albugo candida*.

Supplemental Figure 8. Impaired cellular levels of PI(4,5)P_2 in *pip5k1 pip5k2* mutants.

Supplemental Figure 9. Cellular localization of PIP5K1-YFP and PIP5K2-YFP in Arabidopsis.

Supplemental Figure 10. Expression levels of *PR1*, *PDF1.2a*, and *FRK1* genes in Col-0 wild type and *pip5k1 pip5k2* at 2, 5 and 7 Dys after inoculation with *E. cichoracearum*.

Supplemental Figure 11. Cellular dynamics of MLO2 and reorganization of actin filaments in *pip5k1 pip5k2* mutant.

Supplemental Figure 12. Loss of PIP5K1 and PIP5K2 functions prevented disease development of *C. higginsianum* infection on detached Arabidopsis leaves.

Supplemental Table 1. Frequency of phosphoinositide biosensor accumulation at the extrahaustorial membrane of powdery mildew.

Supplemental Table 2. Oligonucleotide sequences of primers used in this study.

Supplemental Data Set 1. Differentially expressed genes in Col-0 wild type and *pip5k1 pip5k2* at 2, 5 and 7 Dys after inoculation with *E. cichoracearum*.

Supplemental Data Set 2. Statistical analyses performed in this study.

Supplemental Movie 1. Z-stack images showing the spatial distribution of PI4P at the penetration site of powdery mildew *E. cichoracearum*.

Supplemental Movie 2. Z-stack images showing the spatial distribution of PI(4,5)P_2 at the penetration site of powdery mildew *E. cichoracearum*.

Supplemental Movie 3. Z-stack images showing the actin filaments in epidermal cells of Col-0 leaves hosting a mature haustorium of powdery mildew *E. cichoracearum*.

Supplemental Movie 4. Z-stack images showing the actin filaments in epidermal cells of *pip5k1 pip5k2* mutant leaves hosting a mature haustorium of powdery mildew *E. cichoracearum*.

Supplemental Movie 5. Z-stack images of epidermal cells of *pip5k1 pip5k2* mutant leaves inoculated with *C. higginsianum*.

ACKNOWLEDGMENTS

We thank Vipen Sawhney for critically reading the article, Shunyan Xiao and Mohammad H. Borhan for providing materials, and the ABRC (Ohio State University) for providing seeds for T-DNA insertion lines and transgenic marker lines. This work was supported the Natural Sciences and Engineering Research Council of Canada (Discovery Grant), the Canadian Foundation for Innovation (to Y.W.) and the National Natural Science Foundation of China (grant 31471428 to Z.Z.).

AUTHOR CONTRIBUTIONS

L.Q., Z.Z., and Y.W. initiated the project; L.Q., Z.Z., L.L., and Y.W. performed microscopic analyses; L.Q. and Y.W. conducted pathogenicity tests; C.Z., G.P., and L.Q. generated transgenic plants; P.G., R.D., and D.X. measured hormones; Q.L. and D.X. conducted gene expression profiling; L.Q and T.D.Q. performed immunofluorescence; S.A.K. and Y.J. provided experimental materials; L.Q., Z.Z., and Y.W. wrote the article with input from Y.J., S.A.K., R.D., G.P., and D.X.

Received December 16, 2019; revised February 7, 2020; accepted March 9, 2020; published March 10, 2020.

REFERENCES

Anders, S., Pyl, P.T., and Huber, W. (2015). HTSeq: A Python framework to work with high-throughput sequencing data. Bioinformatics **31:** 166–169.

Asai, T., Tena, G., Plotnikova, J., Willmann, M.R., Chiu, W.-L., Gomez-Gomez, L., Boller, T., Ausubel, F.M., and Sheen, J. (2002). MAP kinase signalling cascade in *Arabidopsis* innate immunity. Nature **415:** 977–983.

Berkey, R., Zhang, Y., Ma, X., King, H., Zhang, Q., Wang, W., and Xiao, S. (2017). Homologues of the RPW8 resistance protein are localized to the extrahaustorial membrane that is likely synthesized de novo. Plant Physiol. **173:** 600–613.

Bhat, R.A., Miklis, M., Schmelzer, E., Schulze-Lefert, P., and Panstruga, R. (2005). Recruitment and interaction dynamics of plant penetration resistance components in a plasma membrane microdomain. Proc. Natl. Acad. Sci. USA **102:** 3135–3140.

Bolger, A.M., Lohse, M., and Usadel, B. (2014). Trimmomatic: A flexible trimmer for Illumina sequence data. Bioinformatics **30:** 2114–2120.

Borhan, M.H., Brose, E., Beynon, J.L., and Holub, E.B. (2001). White rust (*Albugo candida*) resistance loci on three Arabidopsis chromosomes are closely linked to downy mildew (*Peronospora parasitica*) resistance loci. Mol. Plant Pathol. **2:** 87–95.

Boudsocq, M., Willmann, M.R., McCormack, M., Lee, H., Shan, L., He, P., Bush, J., Cheng, S.H., and Sheen, J. (2010). Differential innate immune signalling via Ca^{2+} sensor protein kinases. Nature **464:** 418–422.

Capasso, S., and D'Angelo, G. (2019). Imaging lipid metabolism at the Golgi complex. In Intracellular Lipid Transport: Methods and Protocols, G. Drin, ed (New York: Springer), pp. 47–56.

Catanzariti, A.-M., Dodds, P.N., Lawrence, G.J., Ayliffe, M.A., and Ellis, J.G. (2006). Haustorially expressed secreted proteins from flax rust are highly enriched for avirulence elicitors. Plant Cell **18:** 243–256.

Celio, G., Mims, C., and Richardson, E. (2004). Ultrastructure and immunocytochemistry of the host pathogen interface in poinsettia leaves infected with powdery mildew. Can. J. Bot. **82:** 421–429.

Choi, S., Thapa, N., Tan, X., Hedman, A.C., and Anderson, R.A. (2015). PIP kinases define PI4,5P_2 signaling specificity by association with effectors. Biochim. Biophys. Acta **1851:** 711–723.

Cockcroft, S., and Raghu, P. (2018). Phospholipid transport protein function at organelle contact sites. Curr. Opin. Cell Biol. **53:** 52–60.

Colin, L.A., and Jaillais, Y. (2020). Phospholipids across scales: Lipid patterns and plant development. Curr. Opin. Plant Biol. **53:** 1–9.

Consonni, C., Humphry, M.E., Hartmann, H.A., Livaja, M., Durner, J., Westphal, L., Vogel, J., Lipka, V., Kemmerling, B., Schulze-Lefert, P., Somerville, S.C., and Panstruga, R. (2006). Conserved requirement for a plant host cell protein in powdery mildew pathogenesis. Nat. Genet. **38:** 716–720.

Cutler, N.S., Heitman, J., and Cardenas, M.E. (1997). STT4 is an essential phosphatidylinositol 4-kinase that is a target of wortmannin in *Saccharomyces cerevisiae*. J. Biol. Chem. **272:** 27671–27677.

Cutler, S.R., Ehrhardt, D.W., Griffitts, J.S., and Somerville, C.R. (2000). Random GFP:cDNA fusions enable visualization of subcellular structures in cells of *Arabidopsis* at a high frequency. Proc. Natl. Acad. Sci. USA **97:** 3718–3723.

DeBono, A., Yeats, T.H., Rose, J.K., Bird, D., Jetter, R., Kunst, L., and Samuels, L. (2009). *Arabidopsis* LTPG is a glycosylphosphatidylinositol-anchored lipid transfer protein required for export of lipids to the plant surface. Plant Cell **21:** 1230–1238.

Dobin, A., Davis, C.A., Schlesinger, F., Drenkow, J., Zaleski, C., Jha, S., Batut, P., Chaisson, M., and Gingeras, T.R. (2013). STAR: Ultrafast universal RNA-seq aligner. Bioinformatics **29:** 15–21.

El Zawily, A.M., et al. (2014). *FRIENDLY* regulates mitochondrial distribution, fusion, and quality control in Arabidopsis. Plant Physiol. **166:** 808–828.

Feechan, A., Jermakow, A.M., Ivancevic, A., Godfrey, D., Pak, H., Panstruga, R., and Dry, I.B. (2013). Host cell entry of powdery mildew is correlated with endosomal transport of antagonistically acting VvPEN1 and VvMLO to the papilla. Mol. Plant Microbe Interact. **26:** 1138–1150.

Frye, C.A., and Innes, R.W. (1998). An Arabidopsis mutant with enhanced resistance to powdery mildew. Plant Cell **10:** 947–956.

Galán, J.E., and Collmer, A. (1999). Type III secretion machines: Bacterial devices for protein delivery into host cells. Science **284:** 1322–1328.

Galán, J.E., and Zhou, D. (2000). Striking a balance: Modulation of the actin cytoskeleton by *Salmonella*. Proc. Natl. Acad. Sci. USA **97:** 8754–8761.

Geldner, N., Anders, N., Wolters, H., Keicher, J., Kornberger, W., Muller, P., Delbarre, A., Ueda, T., Nakano, A., and Jürgens, G. (2003). The *Arabidopsis* GNOM ARF-GEF mediates endosomal recycling, auxin transport, and auxin-dependent plant growth. Cell **112:** 219–230.

Geldner, N., Dénervaud-Tendon, V., Hyman, D.L., Mayer, U., Stierhof, Y.D., and Chory, J. (2009). Rapid, combinatorial analysis of membrane compartments in intact plants with a multicolor marker set. Plant J. **59:** 169–178.

Gil, F., and Gay, J.L. (1977). Ultrastructural and physiological properties of the host interfacial components of haustoria of *Erysiphe pisi in vivo* and *in vitro*. Physiol. Plant Pathol. **10:** 1–12.

Gillaspy, G.E. (2013). The role of phosphoinositides and inositol phosphates in plant cell signaling. Adv. Exp. Med. Biol. **991:** 141–157.

Gouin, E., Welch, M.D., and Cossart, P. (2005). Actin-based motility of intracellular pathogens. Curr. Opin. Microbiol. **8:** 35–45.

Graber, Z.T., Gericke, A., and Kooijman, E.E. (2014). Phosphatidylinositol-4,5-bisphosphate ionization in the presence of cholesterol, calcium or magnesium ions. Chem. Phys. Lipids **182:** 62–72.

Hahn, M., and Mendgen, K. (2001). Signal and nutrient exchange at biotrophic plant-fungus interfaces. Curr. Opin. Plant Biol. **4:** 322–327.

Hammond, G.R., Fischer, M.J., Anderson, K.E., Holdich, J., Koteci, A., Balla, T., and Irvine, R.F. (2012). PI4P and PI(4,5)P_2 are essential but independent lipid determinants of membrane identity. Science **337:** 727–730.

Hammond, G.R., Machner, M.P., and Balla, T. (2014). A novel probe for phosphatidylinositol 4-phosphate reveals multiple pools beyond the Golgi. J. Cell Biol. **205:** 113–126.

Hammond, G.R., Schiavo, G., and Irvine, R.F. (2009). Immunocytochemical techniques reveal multiple, distinct cellular pools of PtdIns4*P* and PtdIns(4,5)P_2. Biochem. J. **422:** 23–35.

Hammond, G.R.V., Dove, S.K., Nicol, A., Pinxteren, J.A., Zicha, D., and Schiavo, G. (2006). Elimination of plasma membrane phosphatidylinositol (4,5)-bisphosphate is required for exocytosis from mast cells. J. Cell Sci. **119:** 2084–2094.

Hauck, P., Thilmony, R., and He, S.Y. (2003). A *Pseudomonas syringae* type III effector suppresses cell wall-based extracellular defense in susceptible *Arabidopsis* plants. Proc. Natl. Acad. Sci. USA **100:** 8577–8582.

He, P., Shan, L., Lin, N.C., Martin, G.B., Kemmerling, B., Nürnberger, T., and Sheen, J. (2006). Specific bacterial suppressors of MAMP signaling upstream of MAPKKK in *Arabidopsis* innate immunity. Cell **125:** 563–575.

Heath, M.C. (1997). Signalling between pathogenic rust fungi and resistant or susceptible host plants. Ann. Bot. **80:** 713–720.

Heilmann, M., and Heilmann, I. (2015). Plant phosphoinositides: Complex networks controlling growth and adaptation. Biochim. Biophys. Acta **1851:** 759–769.

Hempel, F., Stenzel, I., Heilmann, M., Krishnamoorthy, P., Menzel, W., Golbik, R., Helm, S., Dobritzsch, D., Baginsky, S., Lee, J., Hoehenwarter, W., and Heilmann, I. (2017). MAPKs influence pollen tube growth by controlling the formation of phosphatidylinositol 4,5-bisphosphate in an apical plasma membrane domain. Plant Cell **29:** 3030–3050.

Hruz, T., Laule, O., Szabo, G., Wessendorp, F., Bleuler, S., Oertle, L., Widmayer, P., Gruissem, W., and Zimmermann, P. (2008). Genevestigator v3: A reference expression database for the meta-analysis of transcriptomes. Adv. Bioinformatics **2008:** 420747.

Inada, N., Betsuyaku, S., Shimada, T.L., Ebine, K., Ito, E., Kutsuna, N., Hasezawa, S., Takano, Y., Fukuda, H., Nakano, A., and Ueda, T. (2016). Modulation of plant RAB GTPase-mediated membrane trafficking pathway at the interface between plants and obligate biotrophic pathogens. Plant Cell Physiol. **57:** 1854–1864.

Ischebeck, T., Stenzel, I., and Heilmann, I. (2008). Type B phosphatidylinositol-4-phosphate 5-kinases mediate *Arabidopsis* and *Nicotiana tabacum* pollen tube growth by regulating apical pectin secretion. Plant Cell **20:** 3312–3330.

Ischebeck, T., Stenzel, I., Hempel, F., Jin, X., Mosblech, A., and Heilmann, I. (2011). Phosphatidylinositol-4,5-bisphosphate influences Nt-Rac5-mediated cell expansion in pollen tubes of *Nicotiana tabacum*. Plant J. **65:** 453–468.

Ischebeck, T., Vu, L.H., Jin, X., Stenzel, I., Löfke, C., and Heilmann, I. (2010). Functional cooperativity of enzymes of phosphoinositide conversion according to synergistic effects on pectin secretion in tobacco pollen tubes. Mol. Plant **3:** 870–881.

Ischebeck, T., et al. (2013). Phosphatidylinositol 4,5-bisphosphate influences PIN polarization by controlling clathrin-mediated membrane trafficking in *Arabidopsis*. Plant Cell **25:** 4894–4911.

Ivanov, S., and Harrison, M.J. (2019). Accumulation of phosphoinositides in distinct regions of the periarbuscular membrane. New Phytol. **221:** 2213–2227.

Jelínková, A., Malínská, K., Simon, S., Kleine-Vehn, J., Parezová, M., Pejchar, P., Kubes, M., Martinec, J., Friml, J., Zazímalová, E., and Petrásek, J. (2010). Probing plant membranes with FM dyes: Tracking, dragging or blocking? Plant J. **61:** 883–892.

Jha, S.G., Larson, E.R., Humble, J., Domozych, D.S., Barrington, D.S., and Tierney, M.L. (2018). *Vacuolar Protein Sorting 26C* encodes an evolutionarily conserved large retromer subunit in eukaryotes that is important for root hair growth in *Arabidopsis thaliana*. Plant J. **94:** 595–611.

Jones, D.S., Yuan, J., Smith, B.E., Willoughby, A.C., Kumimoto, E.L., and Kessler, S.A. (2017). MILDEW RESISTANCE LOCUS O function in pollen tube reception is linked to its oligomerization and subcellular distribution. Plant Physiol. **175:** 172–185.

Koh, S., André, A., Edwards, H., Ehrhardt, D., and Somerville, S. (2005). *Arabidopsis thaliana* subcellular responses to compatible *Erysiphe cichoracearum* infections. Plant J. **44:** 516–529.

Krinke, O., Ruelland, E., Valentová, O., Vergnolle, C., Renou, J.-P., Taconnat, L., Flemr, M., Burketová, L., and Zachowski, A. (2007). Phosphatidylinositol 4-kinase activation is an early response to salicylic acid in Arabidopsis suspension cells. Plant Physiol. **144:** 1347–1359.

Krishnamoorthy, P., Sanchez-Rodriguez, C., Heilmann, I., and Persson, S. (2014). Regulatory roles of phosphoinositides in membrane trafficking and their potential impact on cell-wall synthesis and re-modelling. Ann. Bot. **114:** 1049–1057.

Kusano, H., Testerink, C., Vermeer, J.E., Tsuge, T., Shimada, H., Oka, A., Munnik, T., and Aoyama, T. (2008). The *Arabidopsis* phosphatidylinositol phosphate 5-kinase PIP5K3 is a key regulator of root hair tip growth. Plant Cell **20:** 367–380.

Kusch, S., and Panstruga, R. (2017). *mlo*-based resistance: An apparently universal "weapon" to defeat powdery mildew disease. Mol. Plant Microbe Interact. **30:** 179–189.

Kwaaitaal, M., Nielsen, M.E., Böhlenius, H., and Thordal-Christensen, H. (2017). The plant membrane surrounding powdery mildew haustoria shares properties with the endoplasmic reticulum membrane. J. Exp. Bot. **68:** 5731–5743.

Lee, E., Vanneste, S., Pérez-Sancho, J., Benitez-Fuente, F., Strelau, M., Macho, A.P., Botella, M.A., Friml, J., and Rosado, A. (2019). Ionic stress enhances ER-PM connectivity via phosphoinositide-associated SYT1 contact site expansion in *Arabidopsis*. Proc. Natl. Acad. Sci. USA **116:** 1420–1429.

Lee, Y., Kim, Y.W., Jeon, B.W., Park, K.Y., Suh, S.J., Seo, J., Kwak, J.M., Martinoia, E., Hwang, I., and Lee, Y. (2007). Phosphatidylinositol 4,5-bisphosphate is important for stomatal opening. Plant J. **52:** 803–816.

Lefebvre, B., Batoko, H., Duby, G., and Boutry, M. (2004). Targeting of a *Nicotiana plumbaginifolia* H^+-ATPase to the plasma membrane is not by default and requires cytosolic structural determinants. Plant Cell **16:** 1772–1789.

Lenoir, M., and Overduin, M. (2013). PtdIns(4)P signalling and recognition systems. Adv. Exp. Med. Biol. **991:** 59–83.

Littlefield, L.J., and Bracker, C.E. (1970). Continuity of host plasma membrane around haustoria of *Melampsora lini*. Mycologia **62:** 609–614.

Liu, G., Greenshields, D.L., Sammynaiken, R., Hirji, R.N., Selvaraj, G., and Wei, Y. (2007a). Targeted alterations in iron homeostasis underlie plant defense responses. J. Cell Sci. **120:** 596–605.

Liu, G., Ji, Y., Bhuiyan, N.H., Pilot, G., Selvaraj, G., Zou, J., and Wei, Y. (2010). Amino acid homeostasis modulates salicylic acid-associated redox status and defense responses in *Arabidopsis*. Plant Cell **22:** 3845–3863.

Liu, G., Kennedy, R., Greenshields, D.L., Peng, G., Forseille, L., Selvaraj, G., and Wei, Y. (2007b). Detached and attached *Arabidopsis* leaf assays reveal distinctive defense responses against hemibiotrophic *Colletotrichum* spp. Mol. Plant Microbe Interact. **20:** 1308–1319.

Lo Presti, L., Lanver, D., Schweizer, G., Tanaka, S., Liang, L., Tollot, M., Zuccaro, A., Reissmann, S., and Kahmann, R. (2015). Fungal effectors and plant susceptibility. Annu. Rev. Plant Biol. **66:** 513–545.

Love, M.I., Huber, W., and Anders, S. (2014). Moderated estimation of fold change and dispersion for RNA-seq data with DESeq2. Genome Biol. **15:** 550.

Makowski, S.L., Tran, T.T., and Field, S.J. (2017). Emerging themes of regulation at the Golgi. Curr. Opin. Cell Biol. **45:** 17–23.

Matsuoka, K., Bassham, D.C., Raikhel, N.V., and Nakamura, K. (1995). Different sensitivity to wortmannin of two vacuolar sorting signals indicates the presence of distinct sorting machineries in tobacco cells. J. Cell Biol. **130:** 1307–1318.

Mei, Y., Jia, W.-J., Chu, Y.-J., and Xue, H.-W. (2012). *Arabidopsis* phosphatidylinositol monophosphate 5-kinase 2 is involved in root gravitropism through regulation of polar auxin transport by affecting the cycling of PIN proteins. Cell Res. **22:** 581–597.

Micali, C.O., Neumann, U., Grunewald, D., Panstruga, R., and O'Connell, R. (2011). Biogenesis of a specialized plant-fungal interface during host cell internalization of *Golovinomyces orontii* haustoria. Cell. Microbiol. **13:** 210–226.

Miklis, M., Consonni, C., Bhat, R.A., Lipka, V., Schulze-Lefert, P., and Panstruga, R. (2007). Barley MLO modulates actin-dependent and actin-independent antifungal defense pathways at the cell periphery. Plant Physiol. **144:** 1132–1143.

Morejohn, L.C. (1991). The molecular pharmacology of plant tubulin and microtubules. In The Cytoskeletal Basis of Plant Growth and Form, C.W. Loyd, ed (London: Academic), pp. 29–43.

Moseley, J.B., and Goode, B.L. (2006). The yeast actin cytoskeleton: From cellular function to biochemical mechanism. Microbiol. Mol. Biol. Rev. **70:** 605–645.

Mueller-Roeber, B., and Pical, C. (2002). Inositol phospholipid metabolism in Arabidopsis: Characterized and putative isoforms of inositol phospholipid kinase and phosphoinositide-specific phospholipase C. Plant Physiol. **130:** 22–46.

Munnik, T., and Nielsen, E. (2011). Green light for polyphosphoinositide signals in plants. Curr. Opin. Plant Biol. **14:** 489–497.

Munnik, T., and Vermeer, J.E. (2010). Osmotic stress-induced phosphoinositide and inositol phosphate signalling in plants. Plant Cell Environ. **33:** 655–669.

Nakanishi, S., Catt, K.J., and Balla, T. (1995). A wortmannin-sensitive phosphatidylinositol 4-kinase that regulates hormone-sensitive pools of inositolphospholipids. Proc. Natl. Acad. Sci. USA **92:** 5317–5321.

Nelson, B.K., Cai, X., and Nebenführ, A. (2007). A multicolored set of *in vivo* organelle markers for co-localization studies in Arabidopsis and other plants. Plant J. **51:** 1126–1136.

Nielsen, M.E., Feechan, A., Böhlenius, H., Ueda, T., and Thordal-Christensen, H. (2012). *Arabidopsis* ARF-GTP exchange factor, GNOM, mediates transport required for innate immunity and focal accumulation of syntaxin PEN1. Proc. Natl. Acad. Sci. USA **109:** 11443–11448.

Noack, L.C., and Jaillais, Y. (2017). Precision targeting by phosphoinositides: How PIs direct endomembrane trafficking in plants. Curr. Opin. Plant Biol. **40:** 22–33.

Nomura, K., Mecey, C., Lee, Y.-N., Imboden, L.A., Chang, J.H., and He, S.Y. (2011). Effector-triggered immunity blocks pathogen degradation of an immunity-associated vesicle traffic regulator in *Arabidopsis*. Proc. Natl. Acad. Sci. USA **108:** 10774–10779.

Ohtani, Y., Irie, T., Uekama, K., Fukunaga, K., and Pitha, J. (1989). Differential effects of α-, β- and γ-cyclodextrins on human erythrocytes. Eur. J. Biochem. **186:** 17–22.

Opalski, K.S., Schultheiss, H., Kogel, K.H., and Hückelhoven, R. (2005). The receptor-like MLO protein and the RAC/ROP family G-protein RACB modulate actin reorganization in barley attacked by the biotrophic powdery mildew fungus *Blumeria graminis* f.sp. *hordei*. Plant J. **41:** 291–303.

Pertea, M., Pertea, G.M., Antonescu, C.M., Chang, T.-C., Mendell, J.T., and Salzberg, S.L. (2015). StringTie enables improved reconstruction of a transcriptome from RNA-seq reads. Nat. Biotechnol. **33:** 290–295.

Pike, L.J., and Miller, J.M. (1998). Cholesterol depletion delocalizes phosphatidylinositol bisphosphate and inhibits hormone-stimulated phosphatidylinositol turnover. J. Biol. Chem. **273:** 22298–22304.

Platre, M.P., and Jaillais, Y. (2016). Guidelines for the use of protein domains in acidic phospholipid imaging. Methods Mol. Biol. **1376:** 175–194.

Pollard, T.D. (2007). Regulation of actin filament assembly by Arp2/3 complex and formins. Annu. Rev. Biophys. Biomol. Struct. **36:** 451–477.

Richter, S., Kientz, M., Brumm, S., Nielsen, M.E., Park, M., Gavidia, R., Krause, C., Voss, U., Beckmann, H., Mayer, U., Stierhof, Y.D., and Jürgens, G. (2014). Delivery of endocytosed proteins to the cell-division plane requires change of pathway from recycling to secretion. eLife **3:** e02131.

Roberts, A.M., Mackie, A.J., Hathaway, V., Callow, J.A., and Green, J.R. (1993). Molecular differentiation in the extrahaustorial membrane of pea powdery mildew haustoria at early and late stages of development. Physiol. Mol. Plant Pathol. **43:** 147–160.

Saarikangas, J., Zhao, H., and Lappalainen, P. (2010). Regulation of the actin cytoskeleton-plasma membrane interplay by phosphoinositides. Physiol. Rev. **90:** 259–289.

Scheler, B., Schnepf, V., Galgenmüller, C., Ranf, S., and Hückelhoven, R. (2016). Barley disease susceptibility factor RACB acts in epidermal cell polarity and positioning of the nucleus. J. Exp. Bot. **67:** 3263–3275.

Schmidt, S.M., and Panstruga, R. (2007). Cytoskeleton functions in plant-microbe interactions. Physiol. Mol. Plant Pathol. **71:** 135–148.

Senju, Y., and Lappalainen, P. (2019). Regulation of actin dynamics by PI(4,5)P_2 in cell migration and endocytosis. Curr. Opin. Cell Biol. **56:** 7–13.

Shimada, T.L., Betsuyaku, S., Inada, N., Ebine, K., Fujimoto, M., Uemura, T., Takano, Y., Fukuda, H., Nakano, A., and Ueda, T. (2019). Enrichment of phosphatidylinositol 4,5-bisphosphate in the extra-invasive hyphal membrane promotes *Colletotrichum* infection of *Arabidopsis thaliana*. Plant Cell Physiol. **60:** 1514–1524.

Simon, M.L., Platre, M.P., Assil, S., van Wijk, R., Chen, W.Y., Chory, J., Dreux, M., Munnik, T., and Jaillais, Y. (2014). A multi-colour/multi-affinity marker set to visualize phosphoinositide dynamics in *Arabidopsis*. Plant J. **77:** 322–337.

Simon, M.L., Platre, M.P., Marquès-Bueno, M.M., Armengot, L., Stanislas, T., Bayle, V., Caillaud, M.-C., and Jaillais, Y. (2016). A PtdIns(4)P-driven electrostatic field controls cell membrane identity and signalling in plants. Nat. Plants **2:** 16089.

Sousa, E., Kost, B., and Malhó, R. (2008). *Arabidopsis* phosphatidylinositol-4-monophosphate 5-kinase 4 regulates pollen tube growth and polarity by modulating membrane recycling. Plant Cell **20:** 3050–3064.

Spector, I., Shochet, N.R., Kashman, Y., and Groweiss, A. (1983). Latrunculins: Novel marine toxins that disrupt microfilament organization in cultured cells. Science **219:** 493–495.

Spencer-Phillips, P., and Gay, J. (1981). Domains of ATPase in plasma membranes and transport through infected plant cells. New Phytol. **89:** 393–400.

Stanislas, T., Hüser, A., Barbosa, I.C., Kiefer, C.S., Brackmann, K., Pietra, S., Gustavsson, A., Zourelidou, M., Schwechheimer, C., and Grebe, M. (2015). *Arabidopsis* D6PK is a lipid domain-dependent mediator of root epidermal planar polarity. Nat. Plants **1:** 15162.

Stenzel, I., Ischebeck, T., König, S., Hołubowska, A., Sporysz, M., Hause, B., and Heilmann, I. (2008). The type B phosphatidylinositol-4-phosphate 5-kinase 3 is essential for root hair formation in *Arabidopsis thaliana*. Plant Cell **20:** 124–141.

Tan, X., Thapa, N., Choi, S., and Anderson, R.A. (2015). Emerging roles of PtdIns(4,5)P_2: Beyond the plasma membrane. J. Cell Sci. **128:** 4047–4056.

Tejos, R., Sauer, M., Vanneste, S., Palacios-Gomez, M., Li, H., Heilmann, M., van Wijk, R., Vermeer, J.E., Heilmann, I., Munnik, T., and Friml, J. (2014). Bipolar plasma membrane distribution of phosphoinositides and their requirement for auxin-mediated cell polarity and patterning in *Arabidopsis*. Plant Cell **26:** 2114–2128.

Toker, A. (1998). The synthesis and cellular roles of phosphatidylinositol 4,5-bisphosphate. Curr. Opin. Cell Biol. **10:** 254–261.

Trapnell, C., Roberts, A., Goff, L., Pertea, G., Kim, D., Kelley, D.R., Pimentel, H., Salzberg, S.L., Rinn, J.L., and Pachter, L. (2012). Differential gene and transcript expression analysis of RNA-seq experiments with TopHat and Cufflinks. Nat. Protoc. **7:** 562–578.

Tsuda, K., Mine, A., Bethke, G., Igarashi, D., Botanga, C.J., Tsuda, Y., Glazebrook, J., Sato, M., and Katagiri, F. (2013). Dual regulation of gene expression mediated by extended MAPK activation and salicylic acid contributes to robust innate immunity in *Arabidopsis thaliana*. PLoS Genet. **9:** e1004015.

van Leeuwen, W., Vermeer, J.E., Gadella, T.W., Jr., and Munnik, T. (2007). Visualization of phosphatidylinositol 4,5-bisphosphate in the plasma membrane of suspension-cultured tobacco BY-2 cells and whole Arabidopsis seedlings. Plant J. **52:** 1014–1026.

van Meer, G., Voelker, D.R., and Feigenson, G.W. (2008). Membrane lipids: Where they are and how they behave. Nat. Rev. Mol. Cell Biol. **9:** 112–124.

Vermeer, J.E., Thole, J.M., Goedhart, J., Nielsen, E., Munnik, T., and Gadella, T.W., Jr. (2009). Imaging phosphatidylinositol 4-phosphate dynamics in living plant cells. Plant J. **57:** 356–372.

Vermeer, J.E., van Leeuwen, W., Tobeña-Santamaria, R., Laxalt, A.M., Jones, D.R., Divecha, N., Gadella, T.W., Jr., and Munnik, T. (2006). Visualization of PtdIns3P dynamics in living plant cells. Plant J. **47:** 687–700.

Voegele, R.T., and Mendgen, K. (2003). Rust haustoria: Nutrient uptake and beyond. New Phytol. **159:** 93–100.

Wang, W., Devoto, A., Turner, J.G., and Xiao, S. (2007). Expression of the membrane-associated resistance protein RPW8 enhances basal defense against biotrophic pathogens. Mol. Plant Microbe Interact. **20:** 966–976.

Wang, W., Wen, Y., Berkey, R., and Xiao, S. (2009). Specific targeting of the *Arabidopsis* resistance protein RPW8.2 to the interfacial membrane encasing the fungal haustorium renders broad-spectrum resistance to powdery mildew. Plant Cell **21:** 2898–2913.

Wang, Y.S., Yoo, C.M., and Blancaflor, E.B. (2008). Improved imaging of actin filaments in transgenic *Arabidopsis* plants expressing a green fluorescent protein fusion to the C- and N-termini of the fimbrin actin-binding domain 2. New Phytol. **177:** 525–536.

Williams, M.E., Torabinejad, J., Cohick, E., Parker, K., Drake, E.J., Thompson, J.E., Hortter, M., and Dewald, D.B. (2005). Mutations in the Arabidopsis phosphoinositide phosphatase gene *SAC9* lead to overaccumulation of PtdIns(4,5)P_2 and constitutive expression of the stress-response pathway. Plant Physiol. **138:** 686–700.

Yang, G., Tang, L., Gong, Y., Xie, J., Fu, Y., Jiang, D., Li, G., Collinge, D.B., Chen, W., and Cheng, J. (2018). A cerato-platanin protein SsCP1 targets plant PR1 and contributes to virulence of *Sclerotinia sclerotiorum*. New Phytol. **217:** 739–755.

Yang, L., Qin, L., Liu, G., Peremyslov, V.V., Dolja, V.V., and Wei, Y. (2014). Myosins XI modulate host cellular responses and penetration resistance to fungal pathogens. Proc. Natl. Acad. Sci. USA **111:** 13996–14001.

Yi, M., and Valent, B. (2013). Communication between filamentous pathogens and plants at the biotrophic interface. Annu. Rev. Phytopathol. **51:** 587–611.

Zhang, X., Henriques, R., Lin, S.-S., Niu, Q.-W., and Chua, N.-H. (2006). *Agrobacterium*-mediated transformation of *Arabidopsis thaliana* using the floral dip method. Nat. Protoc. **1:** 641–646.